UNIVERSIDADE DE SÃO PAULO

ESCOLA POLIÉCNICA

FABIO RIZZA

Reduced-order model of a vertical riser under heave-imposed motion

São Paulo
2014

FABIO RIZZA

Reduced-order model of a vertical riser under heave-imposed motion

Trabalho de Formatura
apresentado à Escola Politécnica
daUniversidade
de São Paulo

Área de concentração:
Engenharia de Estruturas

Orientador: Prof. Dr. Carlos
Eduardo Nigro Mazzilli

Rizza, Fabio
Reduced-order model of a vertical riser under heave-imposed motion / F. Rizza. -- São Paulo, 2015.
47 p.

Trabalho de Formatura - Escola Politécnica da Universidade de São Paulo. Departamento de Engenharia de Estruturas e Geotécnica.

1.Tubulações 2.Método dos elementos finitos I.Universidade de São Paulo. Escola Politécnica. Departamento de Engenharia de Estruturas e Geotécnica II.t.

ABSTRACT

The dynamic behavior of vertical rigid risers under top imposed motion (heave) is considered using a reduced-order model (ROM) based on a Bessel-like mode. Heave motion enforce modulation of the tension amplitude along the riser. In this scenario it will be studied the particular case of parametric resonance caused by an excitation frequency that is equal to the double of the structure's first lateral natural frequency. The vibration modes of slender beams subjected to axial loads (Bessel-like modes) are used to project (via the Galerkin Method) the continuum system dynamics onto a single-degree-of-freedom system phase plane. Then the amplitudes of the response are obtained via numerical integration (Runge-Kutta method family). The ROM obtained will be set according to the experimental results obtained with a physically-reduced model tested in a towing tank (Technological Research Institute of the State of São Paulo, IPT) [1] [2]. A comparison in terms of amplitudes between the ROM based on the Bessel-like modes and the ROM based on trigonometric function is carried out .In order to ensure the correctness and the reliability of the reduced-order model a Finite Element Model develop with a specialized commercial software frequently used in Offshore Engineering (Orcaflex©). Finally, a discussion of the results is made.

CONTENTS

1 CHAPTER 1

This chapter gives a general overview of the offshore structures briefly describing the various types of existing platforms and a specific component of them, the riser, which is the element under investigation in this dissertation.

1.1 INTRODUCTION

Since decades, petroleum companies have been on a constant look out for availability of fossil fuels reserves around the globe. When the land reserves were getting emptied up due to the constant scooping and drilling, the ever increasing demand of oil and gas pushed oil and gas companies further away from the marine coasts into ultra-deep ocean's waters

Huge oil and gas fields were discovered in water depths above $1900\ [m]$ at $250\ [Km]$ off the Brazilian Southeast coast (Lula field, Santos Basin). The reservoirs, estimated between 5 and 8 billion barrels of top quality petroleum, are in the so-called pre-salt layer about $5000\ [m]$ below the sea bottom.

An offshore platform is a large structure with facilities to drill wells, to extract and process oil and natural gas, or to temporarily store product until it can be brought to shore for refining and marketing. . The first offshore platform was installed in 1947 in $6[m]$ depth water. Today there are over 700 units in water depths up to $2000\ [m]$ .Depending on the circumstances, the platform can be grouped in two main types namely: fixed platforms and floating platforms.

1.1.1 FIXED PLATFORMS

The fixed platforms are built on concrete and/or steel legs anchored directly onto the seabed. Such platforms are, by virtue of their immobility, designed for very long term and are economically feasible for installation in water depths up to about $520[m]$.

1.1.1.1 JACKET PLATFORMS

The most common types of fixed platforms is the Jacket one (95%of the offshore platforms in the world are jacket designed**).** Their deck is supported by a steel tubular structure having its feet on the seabed. To fix them onto the seabed, the jacket is equipped with thick steel piles of $2[m]$ diameter that can penetrate the sea floor up to $100[m]$ deep to ensure the stability of the whole platform.

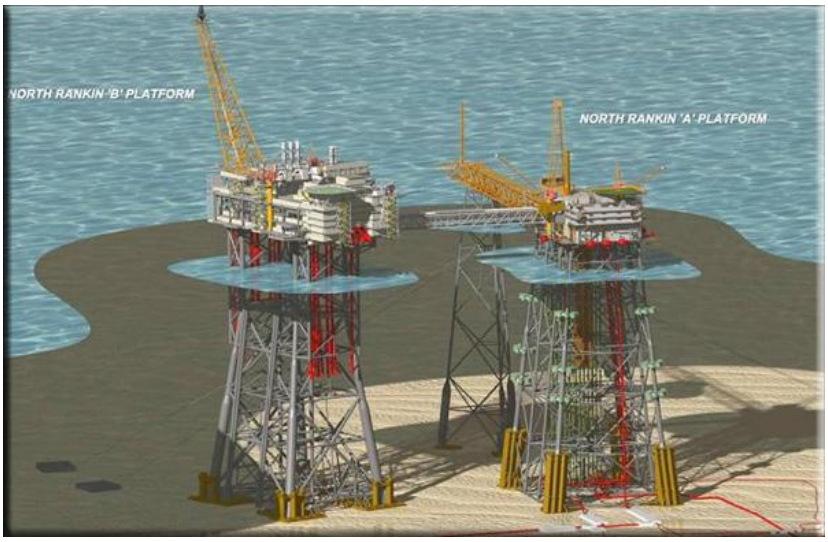

Figure 1: Example of Jacket platform

1.1.2 FLOATING PLATFORMS

Nowadays the design of floating platforms is in continuous development due to the fact that the expected that this is not the limit since fields in $3000[m]$ have already been discovered and obviously the depth can't be reached by fixed platforms.

1.1.2.1 TENSION LEG PLATFORMS

An example of floating platform is the TLP (tension leg platform) used for water depth up to $1200[m]$.They are tied down to the seabed by vertical steel cables called tethers. This characteristic makes the structure very rigid in the vertical direction and very flexible in the horizontal plane. The vertical rigidity helps to tie in wells for production, while, the horizontal compliance makes the platform insensitive to the primary effect of waves. These kinds of oil platforms are highly suitable

in areas prone to regular volatility of the oceanic conditions. Examples of some of the high seas where TLP platforms are currently operated include the Gulf of Mexico and in certain parts of the North Sea. The vertical motion, resisted by the tendons, is not large as compared to the horizontal one; however it causes axial deformations that lead to periodic normal force variations. The main disadvantage of these types of platform is the high initial cost.

Figure 2: Example of Tension Leg Platform

1.1.2.2 SEMI-SUBMERSIBLE PLATFORMS

A semi-submersible platform is designed with a platform-type deck supported by pontoon-type columns that are submerged into the water. They are used for ultra-deep water and are held in place by anchors connected to a catenary mooring system. As a semisubmersible, the rig offers exceptional stability for drilling operation, since rolling and pitching from waves and wind are great diminished. Because semisubmersible platform can float, transporting these rigs from location to location is relatively simple

Figure 3: Example of semi-submersible platform

1.1.2.3 SPAR PLATFORMS

SPAR is a recent type of floating platform (the first spar platform Neptune was installed off the USA in 1997) used for drilling wells beyond $2300[m]$. It is designed with a hollow vertical cylindrical hull and it is secured to the ocean floor by a complex network of cables and tendons. The weight of the cylindrical hull stabilizes the drilling platform and caters for the drilling risers to descend up to the drilling well on the sea floor. The vertical displacement of this type of structure is strongly reduced minimizing in that way the effects of the superficial waves, but is sensitive to problems related to VIV (vortex-induce vibrations)

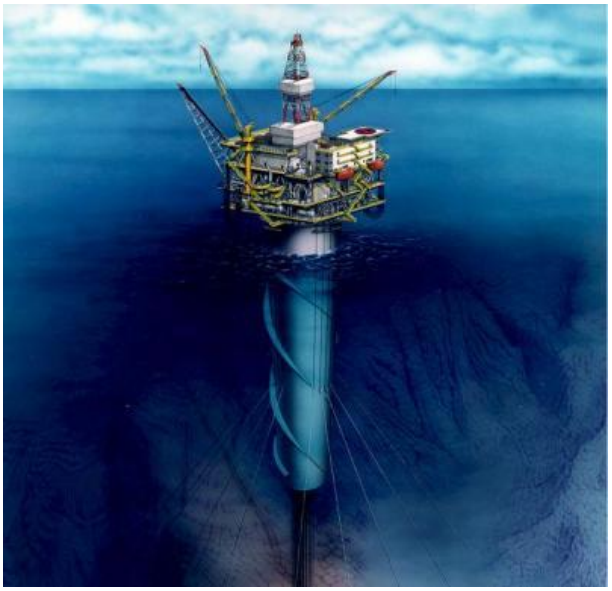

Figure 4: Example of SPAR platform

1.1.2.4 FLOATING OFFSHORE PRODUCTION SYSTEMS

The FPSO (Floating Production Storage and Offloading) system is used extensively by oil companies for the purpose of storing oil from the oil rigs in the middle of the ocean and in the high seas and can be used where building fixed platform and piping is technically and economically not feasible. It is one of the best devised systems developed by the oil exploration industry for deep-water areas.

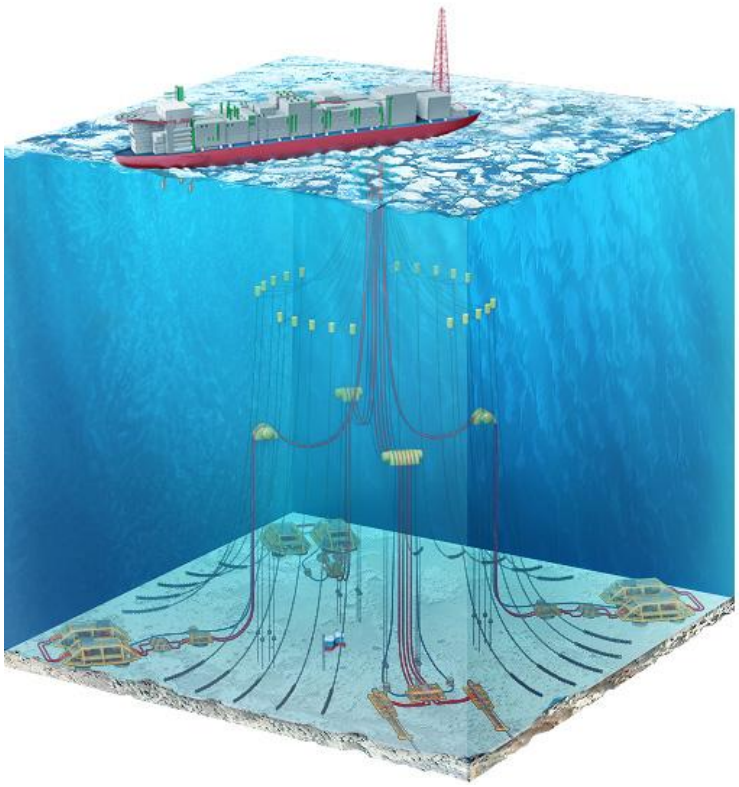

Figure 5 Example of Floating Production Storage and Offloading

The FPSO allows not just storing oil but also producing or refining it before finally offloading it to the desired industrial sectors, either by way of cargo containers or with the help of pipelines built underwater. The use of this system ensures that shipping companies do not have to invest even more money by ferrying the raw and crude oil to an onshore refinery before transferring it to the required industrial areas. In simple terms, the FPSO saves time and money effectively (some of the famous FPSOs are Maersk's FPSOs, Munin Award Winning FPSO, and Shell's Prelude). The FPSO presents 6 degrees of freedom that are showed in the following picture

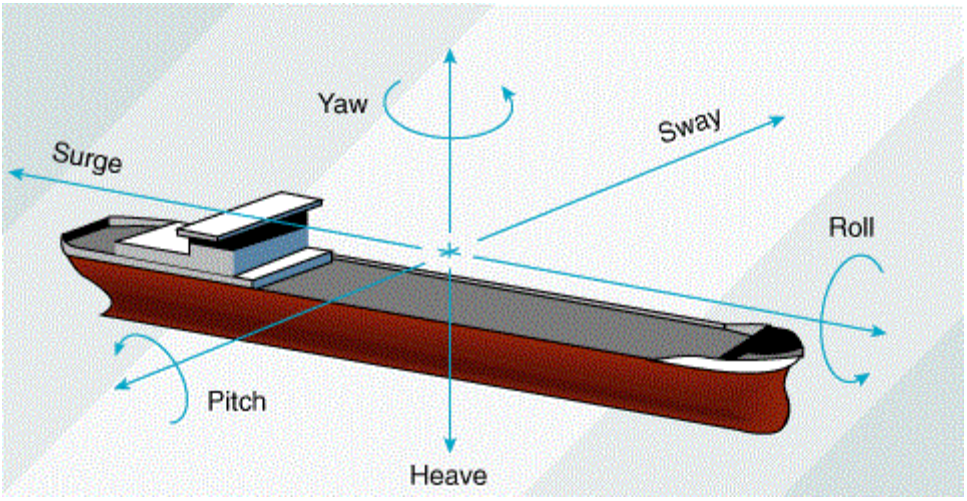

Figure 6: FPSO's degrees of freedom

The displacement imposed by the vessel to the risers can be very large and can cause various problems to the submerged risers and this aspect should be taken into account.

1.1.3 RISERS

In order to convey the hydrocarbon to the sea level, a pipe, conventionally referred to as a riser, is installed between wellhead at the sea bed and the floating platform. Offshore production risers are very slender structures and also a key issue in the design of offshore structure in particular for the service life evaluation of the material due to fatigue. The risers are subjected to large axial thrusts at the top to account for the riser submerged weight, still avoiding undesirable compression at the bottom they are top tensioned.

We can distinguish two typologies of risers namely: flexible and rigid. There are also different kinds of riser configurations, and both flexible risers and rigid risers can be used in free hanging or in a vertical straight configuration.

1.1.3.1 FLEXIBLE RISERS

Flexible risers cope with vessel motion due to wave loading and compensate heave motion (simple catenary risers is freely suspended between surface vessel and the seabed). They are more complex compared to the rigid one because they are made of different material layers, which have specifically structural or operational functions as show in the picture

Figure 7: Flexible riser

1.1.3.2 RIGID RISERS

What are called rigid risers are actually steel tubes. Top-tensioned risers are a completely vertical riser system that terminates directly below the facility. Although moored, these floating facilities are able to move laterally with the wind and waves. Because the rigid risers are also fixed to the seafloor, vertical displacement occurs between the top of the riser and its connection point on the facility. Despite a number of advantages of the straight top-tensioned riser over the catenary riser, straight production risers have not been used yet in water depths over $2000[m]$.

The concern, that is stopping the offshore industry from using top-tensioned straight risers in deep waters, is associated with fluctuation of the axial tension in the riser that is caused by vertical motion (heave) of the platform in waves. Although this fluctuation is significantly reduced by heave compensators, through which the riser is connected to the platform, it can be dangerous. The danger is that the fluctuating tension might destabilize the straight equilibrium of the riser and cause it to vibrate at a dangerously high level.

The vibrations cause stresses in the risers, which may result in fatigue problems from cyclic loads. When considering the fluctuation of top tension in the riser, the parametric instability problem of the riser needs to be addressed first. Besides this, the riser will suffer considerable wave-induced vibration (WIV) and vortex-induced vibration (VIV), which can last for almost the whole design life in harsher environments.

Figure 8: Rigid riser

2 CHAPTER 2

The main theoretical tools (non-linear modes, non-linear Galerkin method) used for the reduce-order model development are here proposed. It is also given the theoretical base of the parametric resonance problem which, in this work, is studied as a possible scenario of risers under heave imposed motion due to the variation of their stiffness that is related to the axial force modification caused by the riser vibration.

2.1 NON-LINEAR MODES

Clearly, linearity is an idealization, an exception to the rule; nonlinearity is a frequent occurrence in real-life applications and the behavior of the risers is an example. The dynamic analysis of riser is strongly non-linear in fact it involves: large displacements in a slender structure; unilateral contact with the seabed (for catenary risers), fluid-structure interaction, vortex-induced vibrations (VIV) etc.

The concept of a normal mode is central in the theory of linear vibrating systems. Any attempt to apply traditional linear analysis to nonlinear systems results, at best, in a suboptimal design. Thus, there is a need for efficient, analytically rigorous, broadly applicable analysis techniques for nonlinear structural dynamics.

During the normal mode motion of a linear conservative system (LNM), each system component moves with the same frequency and with a fixed ratio amongst the displacements of the components. Targeting a straightforward nonlinear extension of the LNM concept, Rosenberg [1] defined a nonlinear mode NNM as a vibration in unison of the system (i.e., a synchronous oscillation). This definition requires that all material points of the system reach their extreme values and pass through zero simultaneously and allows all displacements to be expressed in terms of a single reference displacement. An extension of NNM definition to a broader class of problems, such as non-proportionally damped system for which NNMs are not synchronous motions, was proposed by Shaw and Pierre [2] Yet, for the purposes of the present work, Rosenberg's definition suffices.

It is largely accepted that non-linear modes of vibration may be particularly suitable for obtaining reduced-order models (ROM) in non-linear dynamics, for their ability to grasp, even when just a few of them are taken into account, the essential qualitative system information that a much larger number of linear modes is required to. Thus the main advantage of using the nonlinear modes in comparison with the linear ones is the possibility of obtaining a better ROM with fewer degrees of freedom

However it should be remembered that in nonlinear problems we don't have the guarantee of uniqueness of solutions and different solutions can coexist; they could manifest depending on the parameters perturbation or on the initial conditions

Reduced-order models can be obtained from the modal relations and equations of selected non-linear modal oscillators. In order to determinate the equivalent modal forces we can impose equality between the virtual work in the original phase space and in the reduced order model phase space. The forced nonlinear oscillator's differential equation can be analytically integrated using a perturbation method or numerically in order to obtain the time domain responses. In this dissertation it will be used the Dorman Prince method (RKDP) to integrate analytically the nonlinear differential equation.

2.2 PARAMETRIC RESONANCE

Several sources of nonlinearities are present in the riser analysis, making it a very complex system to study. The nature and amount of dynamic loads that the riser is subjected to makes the problem even more complex. One may have combination of platform movements, waves, internal flow, currents acting in different directions, levels and intensities, which in turn trigger VIV (vortex induced vibrations). In the nonlinear scenario of riser's analysis (due to heave, waves, internal flow, VIV etc.), very interesting dynamical phenomenon can occur: the parametric resonances. A parametric excitation differs from direct forcing since the action appears as a time varying modification of a system parameter (in the case of the riser problem this parameter is the stiffness that varies in relation to the axial force modification caused by the riser vibration). Unlike the classical resonance of forced system (that occurs when the excitation frequency is equal or close to a natural frequency of the system) the primary parametric resonance takes place when the external excitation frequency equals twice one of the natural frequencies of the parametrically exited system. Under parametric resonance the equilibrium configuration becomes unstable and the system leaves it (after an arbitrarily small initial disturbance) in the search of a steady-state solution which may or not exist, depending on the system nonlinear stiffness and/or damping [3] For all the previous reasons it is clear how important is the study of the parametrically resonant scenario in the riser's analysis.

Parametric excitation can be better understood considering the so-called Mathieu equation [4]:

$$\ddot{x} + (\delta + 2\epsilon\, cos2t)\, x = 0 \qquad \textbf{(2.1)}$$

This is a linear undamped equation of motion where the stiffness varies with time. Here the term $cos2t$ acts as an energy source and it is this term that parametrically excite the system

The parameter δ is defined as the quadratic ratio between twice the natural frequency ω and the forcing frequency Ω and ϵ is related to the forcing amplitude

$$\delta = \left(\frac{2\omega}{\Omega}\right)^2 \qquad \textbf{(2.2)}$$

For different values of δ, ϵ the solution can grow without bound or be limited. The Strutt's diagram (Fig.9) indicates the regions where the solution is unbounded (hatched areas), and when parametric

instability is said to occur. Clearly when nonlinearities and dissipative effects are taken into account, as in the case studied, the instability zones change and post-critical steady states may exist.

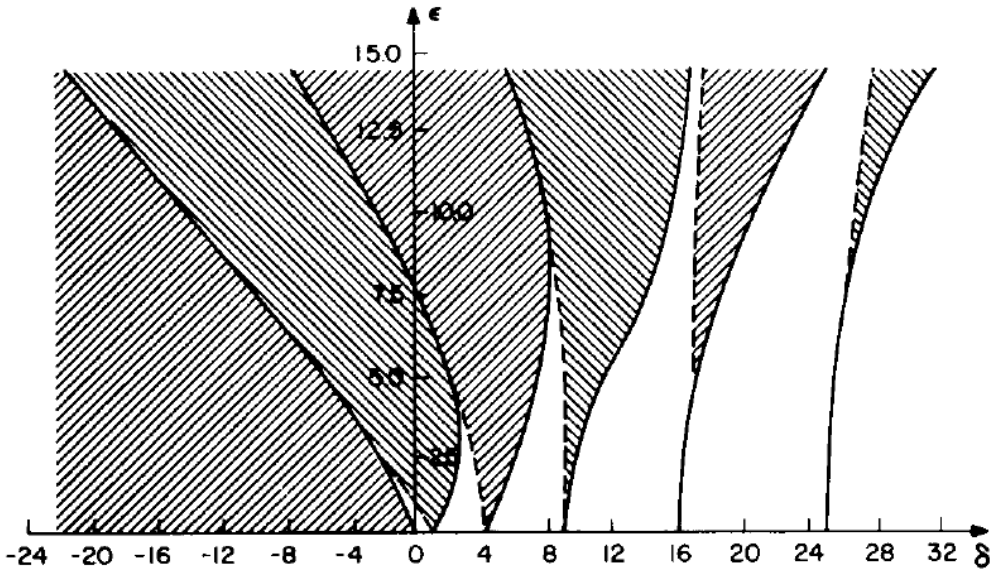

Figure 9: Strutt's diagram (Nayfeh and Mook, 1979)

2.3 NON-LINEAR GALERKIN METHOD

To transform the continuum model into a reduced-order model (ROM) with only one degree of freedom, in the in the following sections the nonlinear Galerkin method [5] [6] will be used.

The nonlinear Galerkin method requires that the virtual work in the 'high-order' model should be equal to that in the reduced-order model. Such equality corresponds to a constraint equation, namely that the virtual work, or the 'energy', imparted to the modes excluded from the 'reduced-order' model should be zero, which, of course, is not an exact statement and in the case studied is like confer all the energy to the first mode:

$\delta W = \delta p^T F_p = \delta U^T F_U$	**(2.3)**

where p and U stand for generalized displacements of the 'high-order' and the 'reduced-order' model and in the same way F_p**,** F_U are the generalized forces each one associated to its model.

To achieve this each terms of the equation(**3.60**) will be interpreted as a force per unit mass and as a result it will be imposed that the virtual work of these "forces per unit mass", defined in the continuous system and evaluated by multiplication by the virtual "displacements" δp, should be equal to the corresponding virtual work of the "modal forces per unit mass" in the reduced-order model, evaluated by multiplication by the virtual "modal displacements" δU.

3 CHAPTER 3

Starting from the Euler-Bernoulli beam theory and using the Hamilton's Principle the transversal displacement equation is obtained. Then the non-linear free vibration of the vertical riser and the relevant Bessel-like mode are provided. The last is used to project via the Galerkin method the continuum dynamics system onto a single degree of freedom system phase plane in order to obtain the reduced-order model for heave.

3.1 RISER MODELLING

This chapter presents the main steps for dimensional formulation of the motion's equation of vertical risers using Hamilton's Principle, so that the transversal motion is de-coupled from the longitudinal one.

In the static configuration the structure is assumed completely vertical and the riser will here modeled as a prestressed slender beam (with constant cross section and made by an homogeneous isotropic material) subjected to an axial force linearly variable over its length due to its submerged weight [7]. Classical simplifying assumptions are made namely: neglecting longitudinal inertial forces and averaging geometric stiffness effects along the beam.

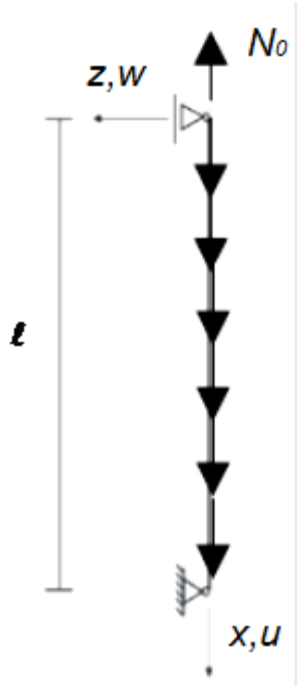

Figure 10: Static configuration of the vertical riser

l beam length

EA axial rigidity

EI bending stiffness

N axial force

$m = \rho A$ mass per unit length

Boundary condition: the axial displacement at $x = l$ is equal to $u_l = 0$ and at the time $t = 0$ in $x = 0$ is imposed an axial displacement namely $-u_0$ due to the prestressed force $N_0(0)$, acting together with the submerged weight.

After the application of $N_0(0)$,the vertical displacement in $x = 0$ will be fixed $u(0,t) = -u_0$ for the purpose of analyzing the vibration modes. However, the axial force in the former region is varying with respect to the time due to the second order bending effects.

In the formulation development it will be adopted the Euler-Bernoulli beam theory

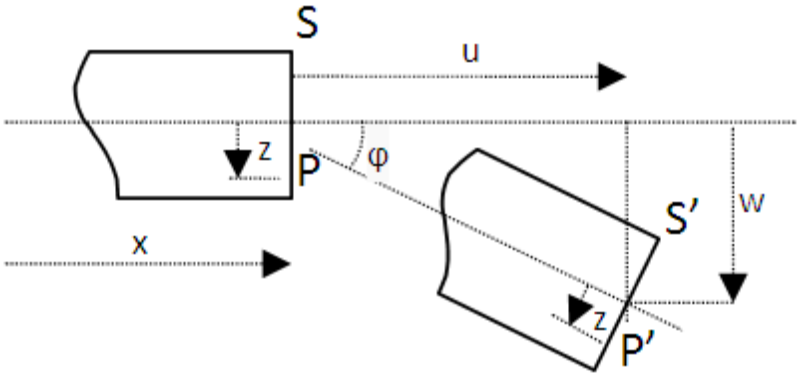

Figure 11: Euler-Bernoulli's kinematics

The generic point displacement will be

$$\begin{aligned} u_p &= u - zsin\varphi \cong u - zw' \\ w_p &= w + z(cos\varphi - 1) \cong w \\ \varphi &= arctan\left(\frac{w'}{1+u'}\right) \cong w' \end{aligned} \quad \textbf{(3.1)}$$

Primes denote differentiation with respect to the axial co-ordinate. The Lagrangian and the engineering strains are assumed to be identical for practical purposes, provided they are small. The strain at a generic point *P* of the riser along the longitudinal direction is

$$\varepsilon_p = u_P' + \frac{1}{2}(u_P')^2 + \frac{1}{2}(w_P')^2 \cong u' - zw'' + \frac{1}{1}(w')^2 = \varepsilon - zw'' \quad \textbf{(3.2)}$$

where ε is the non-linear axial strain at the cross section centroid. Notice that in **(1)** it was assumed that $u_p = 0(w_P^2)$ and the axis strain was introduced as

$$\varepsilon = u' + \frac{1}{2}(w')^2 \tag{3.3}$$

The equations of motion for free vibration will be obtained with Hamilton's principle

$$\int_{t_1}^{t_2} (\delta T - \delta V)\, dt = 0 \tag{3.4}$$

where δT is the kinetic energy variation (neglecting rotational inertia) and δV is the variation of the total potential energy.

The kinetic energy is (where over dots indicate differentiation with respect to time)

$$T = \int_0^l \frac{m}{2}(\dot{u}^2 + \dot{w}^2)dx \tag{3.5}$$

From the former equation, after taking into account the natural boundary conditions,

$$\int_{t_1}^{t_2} \delta T\, dt = -\int_{t_1}^{t_2}\int_0^l m(\ddot{u}\delta u + \ddot{w}\delta w)\, dxdt \tag{3.6}$$

The potential energy is the sum of the internal energy U and the potential energy of conservative forces E_p

$$\int_{t_1}^{t_2} \delta E_p dt = -\int_{t_1}^{t_2}\int_0^l p\delta U\, dxdt \tag{3.7}$$

$$\begin{aligned}\int_{t_1}^{t_2} \delta U = &-\int_{t_1}^{t_2}\int_0^l EA(u'' + w'w'')\,\delta u dxdt - \int_{t_1}^{t_2}\int_0^l EA\left(u''w' + u'w'' + \frac{3}{2}w'^2 w''\right)\delta w dxdt \\ &+ \int_{t_1}^{t_2}\int_0^l EIw^{IV}\,\delta w dxdt\end{aligned} \tag{3.8}$$

As demonstrated in [8], the system of differential equations with coupling between longitudinal and transversal displacement comes out:

$$\begin{cases} m\ddot{u} - EA(u'' + w'w'') - p = 0 \\ m\ddot{w} + EIw^{IV} - EA\left(u''w' + u'w'' + \frac{3}{2}w'^2 w''\right) = 0 \end{cases} \tag{3.9}$$

Neglecting the longitudinal inertial force $m\ddot{u} \cong 0$ we have that the normal force vary linearly along the riser

$$EA\left(u' + \frac{1}{2}w'^2\right)' + p = 0 \tag{3.10}$$

$$EA\left(u' + \frac{1}{2}w'^2\right) + px = N_0(t) \tag{3.11}$$

$$N(x,t) = N_0(t) - px \tag{3.12}$$

At this point, it is more convenient to introduce the average value of normal force $\bar{N}$ calculated at the mid-span (before that the transversal vibrations starts)

$$\bar{N} = -\frac{EAu_0}{l} \tag{3.13}$$

After the riser is expose to bending the normal force in the mid-span is affected by a new term and become

$$-\frac{EAu_0}{l} + \frac{EA}{2l}\int_0^l w'^2 dx \tag{3.14}$$

Thus the axial force at a generic section and generic time will be

$$N(x,t) = \bar{N} + p\left(\frac{l}{2} - x\right) + \frac{EA}{2l}\int_0^l w'^2 dx \tag{3.15}$$

At the top of the riser we have

$$N_0(t) = N(0,t) = \bar{N} + p\frac{l}{2} + \frac{EA}{2l}\int_0^l w'^2 dx = N_0(0) + \frac{EA}{2l}\int_0^l w'^2 dx \tag{3.16}$$

Now it is possible to decouple the transversal displacement equation from the longitudinal one **[7]** to obtaining

$$m\ddot{w} + EIw^{IV} - N(x,t)w'' + pw' = 0 \tag{3.17}$$

$$m\ddot{w} + EIw^{IV} - \left(\frac{EAu_0}{l} + p\left(\frac{l}{2} - x\right) + \frac{EA}{2l}\int_0^l w'^2 dx\right)w'' + pw' = 0 \tag{3.18}$$

Introducing the following parameters:

$$\alpha = \frac{EI}{m}$$

$$\beta = \frac{\overline{N}}{m}$$

$$\gamma = \frac{p}{m} \qquad \textbf{(3.19)}$$

$$\mu = \frac{EA}{2ml}$$

It is finally obtained the transversal displacement equation written in dimensional form

$$\frac{\partial^2 w}{\partial t^2} + \alpha \frac{\partial^4 w}{\partial x^4} - \beta \frac{\partial^2 w}{\partial x^2} - \gamma \left(\frac{1}{2} - x\right) \frac{\partial^2 w}{\partial x^2} + \gamma \frac{\partial w}{\partial x} - \mu \frac{\partial^2 w}{\partial x^2} \int_0^{\ell} \left(\frac{\partial w}{\partial x}\right)^2 \mathrm{d}x = 0 \qquad \textbf{(3.20)}$$

3.2 NON LINEAR FREE VIBRATION

Recalling the transversal displacement equation **(3.18)**

$$m\ddot{w} + EIw^{IV} - \left(\frac{EAu_0}{l} + p\left(\frac{l}{2} - x\right) + \frac{EA}{2l}\int_0^l w'^2 dx\right) w'' + pw' = 0 \qquad \textbf{(3.21)}$$

We change the reference system in order to obtain an equivalent cable equation from the previous one

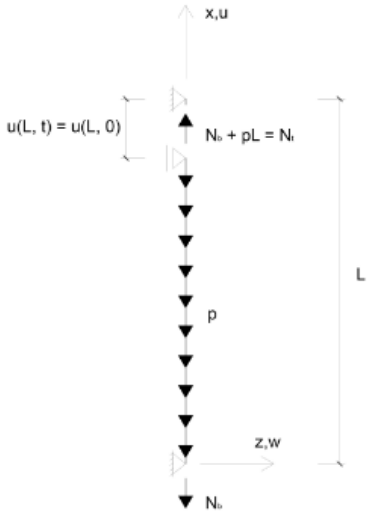

Figure 12: Static configuration of the vertical riser

If the dynamic is dominated by a single mode, as it is supposed to be the case for a riser subjected to a parametric resonance, the solution is searched in the form

$$w(x,t) = W(x)sin\omega t \tag{3.22}$$

And subtitling in **(3.21)** we get

$$EIW^{IV} - N(x)W'' - pW' - \frac{EA}{2L}W''\int_0^L W'^2 \sin^2\omega t dx - m\omega^2 W = 0 \tag{3.23}$$

$$N(x) = \frac{EAu_0}{l} + p\left(\frac{l}{2} - x\right) \tag{3.24}$$

As a second approximation temporal Galerkin projection is applied to **(3.23)** followed by integration over the response period $\frac{2\pi}{\omega}$

$$EIW^{IV} - N(x)W'' - pW' - \frac{3EA}{8L}W''\int_0^L W'^2 dx - m\omega^2 W = 0 \tag{3.25}$$

Defining a fictitious normal force $N^*(x)$ such as

$$EIW^{IV} - \frac{3EA}{8L}W''\int_0^L W'^2 dx = -N^*(x)W'' \tag{3.26}$$

We arrive at a formally equivalent cable equation (with tension $[N^*(x) + N(x)]$)

$$-N^*(x)W'' - N(x)W'' - pW' - m\omega^2 W = 0 \tag{3.27}$$

$$[N^*(x) + N(x)]W'' + pW' + m\omega^2 W = 0 \tag{3.28}$$

The last approximation is the definition of a normal force that comes out from the linear mode

$$W_n(x) = W_{0n}\sin\frac{n\pi x}{L} \tag{3.29}$$

with n that indicates the mode number. We can then compute

$$N^*(x) \cong N_{0_\eta} = \left(\frac{n\pi}{L}\right)^2 EI_{eq} \tag{3.30}$$

where $EI_{eq} = EI\left(1 + \frac{3\eta_n^2}{16}\right)$ and $\frac{3\eta_n^2}{16}$ represents the nonlinear correction due to the motion amplitude[8]

$$\eta_n = \frac{W_{o_n}}{\sqrt{\frac{I}{A}}} = \frac{W_{o_n}}{r} \tag{3.31}$$

$W_{0n}(t) = r\eta(t)$ is the dimensional modal amplitude of the n[th] mode and $\eta(t) = \frac{W_{0n}}{r}$ is the non-dimensional modal amplitude, recalling that the radios of gyration is defined ad $r = \sqrt{\frac{I}{A}}$

Thus the equivalent cable equation becomes

$$\left[N_{0_\eta} + N(x)\right] W'' + pW' + m\omega^2 W = 0 \tag{3.32}$$

And a variable transformation introduced as

$$x = \frac{az^2}{4} - \frac{N_{b_n}}{p} \tag{3.33}$$

$$z = 2\sqrt{\frac{m\left(N_{b_n} + px\right)}{p}}\,\omega_n \tag{3.34}$$

with

$$a = \frac{p}{m\omega_n^2} \tag{3.35}$$

$$N_{b_n} = N_b(0) + N_{0_n} \tag{3.36}$$

so that

$$\frac{d^2W_n}{dz^2} + \frac{1}{z}\frac{dW_n}{dz} + W_n = 0 \tag{3.37}$$

Also, it is defined X_n in such a way that

$$W_n = \frac{1}{\sqrt{z}} X_n \tag{3.38}$$

Leading to an equivalent, yet simpler differential equation

$$\frac{d^2X_n}{dz^2} + \left(1 + \frac{1}{4z^2}\right) X_n = 0 \tag{3.39}$$

Notice that $\frac{1}{4z^2} \ll 1$ and also its average value $2\varepsilon = \frac{1}{z_t - z_b}\int_{z_b}^{z_t} \frac{dz}{4z^2} = \frac{1}{4z_b z_t} \ll 1$

In the expressions above, subscripts z_b and z_t stand for bottom and top.

A familiar equation of motion then appears:

$$\frac{d^2X_n}{dz^2} + (1 + 2\varepsilon)X_n = 0 \tag{3.40}$$

Whose solution is approximately given by

$$X_n(z) \cong C_n \sin\beta_n z + D_n \cos\beta_n z \tag{3.41}$$

Provided

$$\beta_n = \sqrt{1 + 2\varepsilon} \cong 1 + \varepsilon \cong 1 \tag{3.42}$$

From which

$$W_n = \frac{1}{\sqrt{z}}[C_n \sin(z) + D_n \cos(z)] \tag{3.43}$$

Taking into account the boundary conditions

$$W_n(z_b) = W_n(z_t) = 0 \tag{3.44}$$

The following homogenous system comes out [9]

$$\begin{bmatrix} \frac{\sin(z_b)}{\sqrt{z_b}} + \frac{\cos(z_b)}{\sqrt{z_b}} \\ \frac{\sin(z_t)}{\sqrt{z_t}} + \frac{\cos(z_t)}{\sqrt{z_t}} \end{bmatrix} \begin{bmatrix} C_n \\ D_n \end{bmatrix} = \begin{Bmatrix} 0 \\ 0 \end{Bmatrix} \tag{3.45}$$

Requiring that

$$\frac{1}{z_b z_t} \sin(z_t - z_b) = 0 \tag{3.46}$$

$$z_t - z_b = n\pi \tag{3.47}$$

For not-trivial solutions to exist

Defining $C_n = \sqrt{z_b} cos z_b$

$$\begin{cases} \omega_n = \dfrac{n\pi}{2L\sqrt{m}}\left(\sqrt{N_{b_n}} + \sqrt{N_{t_n}}\right) \\ W_n(z) = \sqrt[4]{\dfrac{N_{b_n}}{N_{b_n} + px}}\sin\left(z - z_b\right) \\ z = \dfrac{\sqrt{N_{b_n} + px}}{\sqrt{N_{b_n}} + \sqrt{N_{t_n}}}n\pi \end{cases} \quad \textbf{(3.48)}$$

Combining the equations **(3.48)** is possible to rewrite $W_n(z)$ in the in the following way

$$\psi_n(x,\eta) = (1+ax)^{-\frac{1}{4}} \cdot sin\left[b(\sqrt{1+ax}-1)\right] \quad \textbf{(3.49)}$$

Where

$$a = \frac{P}{T_{bn}} \qquad T_{bn} = T_{b(o)} + \left(\frac{n\pi}{l}\right)^2 EI(1+\frac{3}{16}{\eta_n}^2) \qquad T_{b(o)} = \bar{N} - \frac{pl}{2} \qquad b = \frac{n\pi}{\sqrt{1+al}-1} \quad \textbf{(3.50)}$$

The approximate non-linear solution supplies accurate information regarding the modal shapes that can thus be used as projection functions within the non-linear Galerkin procedure to obtain reduced-order models (ROM). As defined here, these are the Bessel like modes.

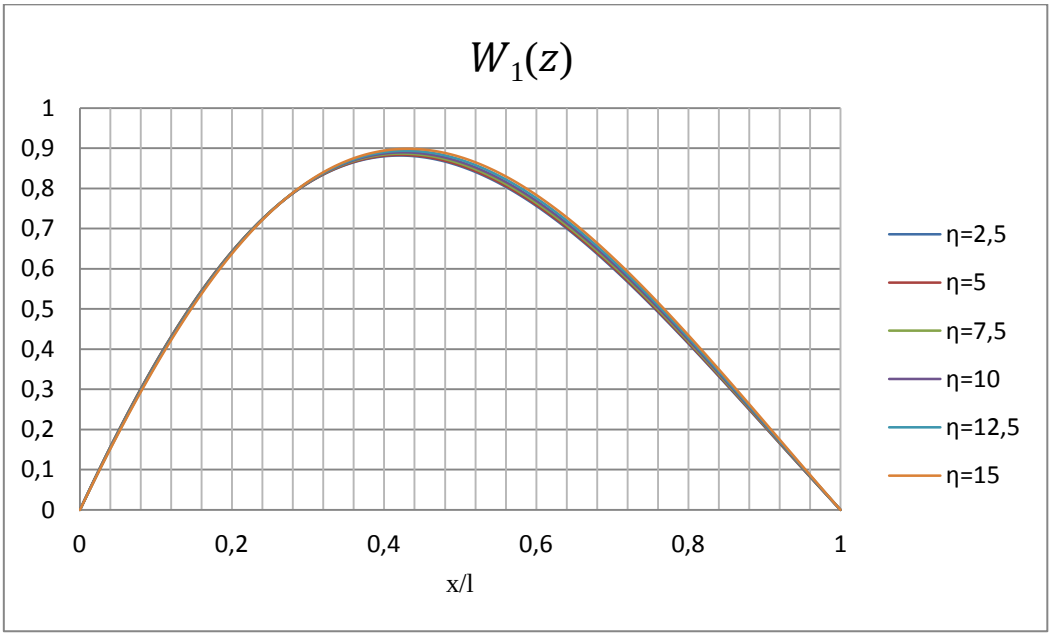

Figure 13: First modal shape with increasing non-linear terms

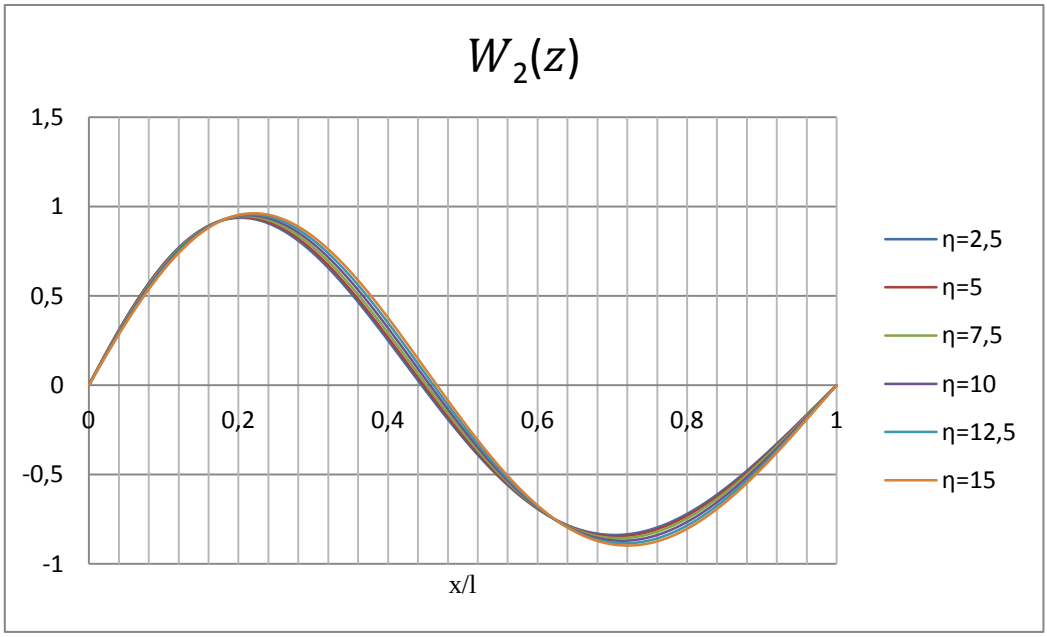

Figure 14: second modal shape with increasing non-linear terms

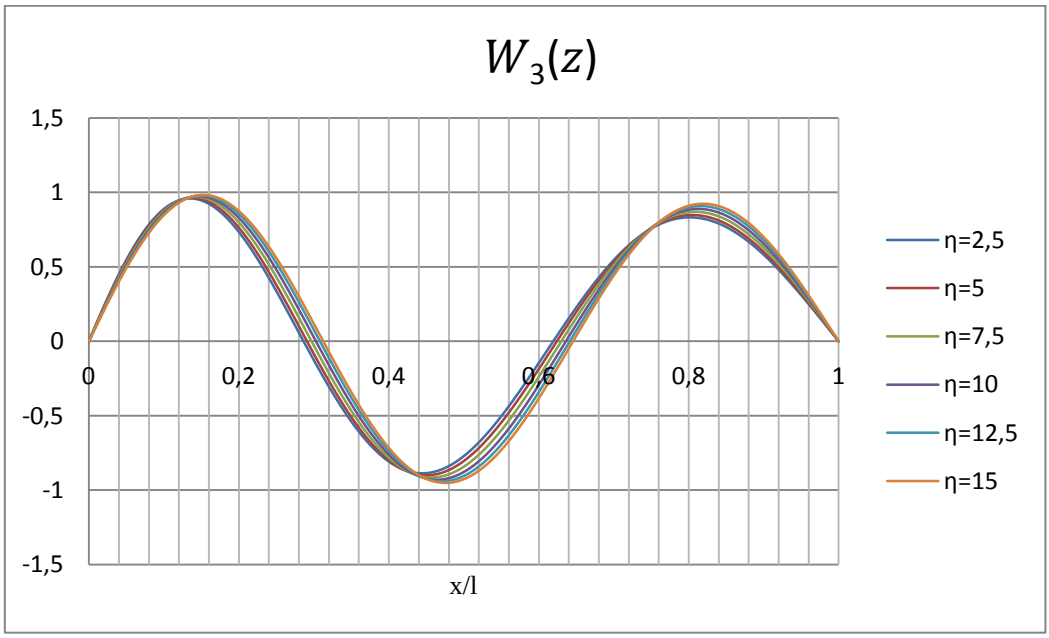

Figure 15: Third modal shape with increasing non-linear terms

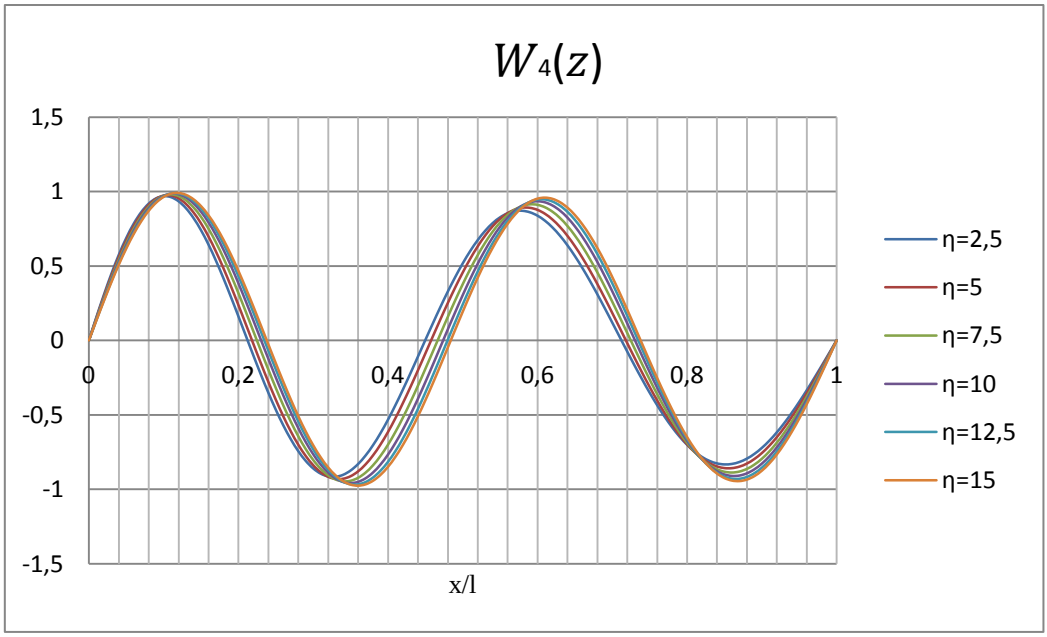

Figure 16: Fourth modal shape with increasing non-linear terms

As shown by the graphs for the first mode, it is possible to neglect de influence of the non-linear correction to the bending stiffness without compromising the quality of the results. This is not true for higher modes, where it is possible to see an increasing shift of the shape caused by the non-linearity correction

$$EI_{eq} = EI\left(1 + \frac{3\eta_n^2}{16}\right) \tag{3.51}$$

3.3 REDUCED-ORDER MODEL FOR HEAVE

Starting with the nonlinear equation for the riser under free vibration is possible to add terms that will consider the effect of the heave sign as a harmonic variation with a forcing frequency that is twice one of the linear natural frequencies of the system (in order to consider the parametric instability scenario). The relevant Bessel-like mode **(3.49)** is used to project via the Galerkin method the continuum dynamics system onto a single degree of freedom system phase plane obtaining a reduced-order model.

Recovering the dimensional equation of the non- linear free oscillator **(3.20)**

$$\frac{\partial^2 w}{\partial t^2} + \alpha \frac{\partial^4 w}{\partial x^4} - \beta \frac{\partial^2 w}{\partial x^2} - \gamma \left(\frac{1}{2} - x\right) \frac{\partial^2 w}{\partial x^2} + \gamma \frac{\partial w}{\partial x} - \mu \frac{\partial^2 w}{\partial x^2} \int_0^{\ell} \left(\frac{\partial w}{\partial x}\right)^2 \mathrm{d}x = 0 \tag{3.52}$$

it is possible to take into account the effect of a vertical imposed top motion (heave) adding a new term, namely $\beta_h(t)$ (the effect of the average axial force $\bar{N}$ along the riser, is already considered by β)

$$\beta_h(t) = \frac{EAh(t)}{m\ell} \tag{3.53}$$

Heave will be sought as a harmonic function

$$h(t) = ho \cdot \cos\left(\hat{\Omega} \cdot \mathrm{t}\right) \tag{3.54}$$

where $\hat{\Omega}$ is the heave frequency $\hat{\Omega} = 2\hat{\omega}_1$ which is twice the first natural frequency in still water ($\hat{\omega}_1$) defined as a ratio between the natural frequency in air of the first non-liner mode ω_1 (with hypothesis of $\bar{N}$ acting all over the riser) and $\sqrt{1 + C_a^*}$ (see equation **(3.70)** for the definition of C_a^* coefficient)

$$\hat{\omega}_1 = \frac{\omega_1}{\sqrt{1 + C_a^*}} \tag{3.55}$$

$$\omega_1 = \frac{\pi}{l} \sqrt{\beta + \frac{\pi^2}{l^2} \alpha} \tag{3.56}$$

Nevertheless the transversal load q_w due to a relative movement fluid-structure movement must be considered (the VIV effect will not be taken into account in this work)

$$\frac{\partial^2 w}{\partial t^2} + \alpha \frac{\partial^4 w}{\partial x^4} - (\beta + \beta_h) \frac{\partial^2 w}{\partial x^2} - \gamma \left(\frac{1}{2} - x\right) \frac{\partial^2 w}{\partial x^2} + \gamma \frac{\partial w}{\partial x} - \mu \frac{\partial^2 w}{\partial x^2} \int_0^{\ell} \left(\frac{\partial w}{\partial x}\right)^2 \mathrm{d}x = \vartheta_w(t) \tag{3.57}$$

$$\vartheta_w(t) = \frac{q_w(t)}{m} \tag{3.58}$$

Where

$$q_w(t) = -C_a \rho_w \frac{\pi D^2}{4} \frac{\partial^2 w}{\partial t^2} - \frac{1}{2} C_d \rho_w D \left| \frac{\partial w}{\partial t} \right| \frac{\partial w}{\partial t} \tag{3.59}$$

$$\frac{\partial^2 w}{\partial t^2} + \alpha \frac{\partial^4 w}{\partial x^4} - (\beta + \beta_h(t)) \frac{\partial^2 w}{\partial x^2} - \gamma \left(\frac{1}{2} - x \right) \frac{\partial^2 w}{\partial x^2} + \gamma \frac{\partial w}{\partial x} - \mu \frac{\partial^2 w}{\partial x^2} \int_0^{\ell} \left(\frac{\partial w}{\partial x} \right)^2 \mathrm{d}x = \\ = -\frac{C_a}{m} \rho_w \frac{\pi D^2}{4} \frac{\partial^2 w}{\partial t^2} - \frac{1}{2} \frac{C_d}{m} \rho_w D \left| \frac{\partial w}{\partial t} \right| \frac{\partial w}{\partial t} \tag{3.60}$$

It should be recalled that the Morison equation is a semi-empirical equation for the inline force on a body in oscillatory flow and it is the sum of two components: an inertia force and a drag force.

$$F = \rho_{fl} C_a \frac{\pi D^2}{4} \ddot{w} + \frac{1}{2} \rho_{fl} C_d D |\dot{w}| \tag{3.61}$$

$$F_I = \rho_{fl} C_a V \ddot{w} \text{ inertia force} \tag{3.62}$$

$$F_D = \tfrac{1}{2} \rho_{fl} C_d A \dot{w} |\dot{w}| \text{ drag force} \tag{3.63}$$

The equation contains two empirical hydrodynamic coefficients: an inertia coefficient (C_a is the added mass coefficient) and a drag coefficient C_d which depends on the Keulegan–Carpenter number, Reynolds number and surface roughness.

The two previous mentioned coefficients are contained as well in $q_w(t)$ **(3.59)**.These coefficients allow to consider: the effects related to the fluid additional mass, due to the distortion of the fluid flow by the presence of the body, namely

$$C_a = \frac{{C_a}^* m}{\frac{\pi D^2}{4} \rho_{fl}} \tag{3.64}$$

and the Morison damping type effects through the drag coefficient C_d.

The coefficient ${C_a}^*$, which stands for the ration between the water added mass per unit length and the riser mass per unit length, and the drag coefficient $C_d$must be calibrated over the experimental results obtained in IPT's experiment

It is more convenient to re-write the obtained equation **(3.60)** in non-dimensional form: with respect to space, by means of the new variable v and ξ, and time which is normalized with respect to the riser first-mode frequency in still water.

$$v = \frac{w}{D} \tag{3.65}$$

$$\xi = \frac{x}{l} \tag{3.66}$$

$$\tau = \widehat{\omega}_1 t \tag{3.67}$$

For the chain rule

$$\frac{\partial v}{\partial x} = \frac{\partial}{\partial \xi} \cdot \frac{d\xi}{dx} = \frac{1}{l} \cdot \frac{\partial v}{\partial \xi} \qquad \frac{\partial^2 v}{\partial x^2} = \frac{1}{l^2} \cdot \frac{\partial^2 v}{\partial \xi^2} \qquad \frac{\partial^4 v}{\partial x^4} = \frac{1}{l^4} \cdot \frac{\partial^4 v}{\partial \xi^4}$$
$$\frac{\partial v}{\partial t} = \frac{\partial}{\partial \tau} \cdot \frac{d\tau}{dt} = \widehat{\omega}_1 \cdot \frac{\partial v}{\partial \tau} \qquad \frac{\partial^2 v}{\partial t^2} = {\widehat{\omega}_1}^2 \cdot \frac{\partial^2 v}{\partial \tau^2} \tag{3.68}$$

yield

$$\begin{aligned} &{\widehat{\omega}_1}^2 \cdot \frac{\partial^2 v}{\partial \tau^2} D + C_a^* \cdot {\widehat{\omega}_1}^2 \cdot \frac{\partial^2 v}{\partial \tau^2} D + a_1^* \left| \widehat{\omega}_1 \cdot \frac{\partial v}{\partial \tau} \right| \widehat{\omega}_1 \cdot \frac{\partial v}{\partial \tau} D^2 + \alpha \frac{1}{l^4} \cdot \frac{\partial^4 v}{\partial \xi^4} D \\ &-\big(\beta + \beta_h(\tau)\big) \frac{1}{l^2} \cdot \frac{\partial^2 v}{\partial \xi^2} D - \gamma l \left(\frac{1}{2} - \xi\right) \frac{1}{l^2} \cdot \frac{\partial^2 v}{\partial \xi^2} D + \gamma \frac{1}{l} \cdot \frac{\partial v}{\partial \xi} \mathrm{D} \\ &-\mu \frac{1}{l^2} \cdot \frac{\partial^2 v}{\partial \xi^2} D \int_0^1 \left(\frac{1}{l} \cdot \frac{\partial v}{\partial \xi} D\right)^2 \mathrm{d}\xi = 0 \end{aligned} \tag{3.69}$$

with the following coefficients

$$a_1^* = \frac{C_d \rho_w D}{2m} \qquad C_a^* = \frac{C_a}{m} \rho_w \frac{\pi D^2}{4} \qquad h(\tau) = ho \cdot \cos\left(\widehat{\Omega} \cdot \frac{\tau}{\widehat{\omega}_1}\right) \tag{3.70}$$

The reduced-order model that will be obtained will use linearized Bessl-like mode within the Galerkin projection, according to two important approximations:

- It will be considered the scenario of parametric resonance with the first mode $n = 1$; as a consequence the whole energy of the continuous system is assumed to be constrained to the first mode
- $T_{b1} = T_b(o) + \left(\frac{\pi}{l}\right)^2 EI \left(1 + \frac{3}{16} {\eta_1}^2\right) \cong T_b(o) + \left(\frac{\pi}{l}\right)^2 EI$, because as seen in the section 3.2, it is possible to assume that the first mode is insensitive to the non-linear correction implied by the term $\frac{3}{16} {\eta_n}^2$in the bending stiffness.

Adopting the usual non-dimensional variables

$$\xi = \frac{x}{l} \qquad \tau = \widehat{\omega}_1 t$$

$$\psi_n(\xi,\eta_n) = (1+al\xi)^{-\frac{1}{4}} \cdot \sin\left[b(\sqrt{1+al\xi}-1)\right] \tag{3.71}$$

$$w_n(\xi,\eta_n,\tau) = W_{0n}(\tau)\frac{\psi_n(\xi,\eta_n)}{\psi_n(\overline{\xi},\eta_n)} = W_{0n}(\tau)\phi(\xi,\eta_n) \tag{3.72}$$

$$w_n(\xi,\eta_n,\tau) = W_{0n}(\tau)\phi(\xi,\eta_n) = r\eta(\tau)\phi(\xi,\eta_n) \tag{3.73}$$

$$v_n(\xi,\eta_n,\tau) = \eta_n(\tau)\frac{r}{D}\phi(\xi,\eta_n) \tag{3.74}$$

where $\overline{\xi}$ indicates the point where the function $\sin\frac{n\pi x}{l}$ exhibits a maximum, namely $\overline{\xi} = \frac{1}{2\pi}$. Consequently $\psi_n(\overline{\xi},\eta)$ is a pure number.

The equation **(3.74)** will be used for projecting via Galerkin method the continuum dynamics system onto a single degree of freedom with $n = 1$ $(\eta_1 = \eta)$

Inserting **(39)** in **(35)** yields

$$\begin{aligned}&\widehat{\omega}_1{}^2 \cdot r\ddot{\eta}\cdot\phi + C_a^*\cdot\widehat{\omega}_1{}^2\cdot r\ddot{\eta}\cdot\phi + a_1^*\cdot|r\dot{\eta}\cdot\widehat{\omega}_1\phi|\cdot r\dot{\eta}\cdot\widehat{\omega}_1\phi + \alpha\frac{1}{l^4}\cdot r\eta\cdot\phi^{IV}\\ &-\frac{(\beta+\beta_h(\tau))}{l^2}\cdot r\eta\cdot\phi^{II} - \frac{\gamma}{l}\left(\frac{1}{2}-\xi\right)\cdot r\eta\cdot\phi^{II} + \frac{\gamma}{l}\cdot r\eta\cdot\phi^{I} - \frac{\mu}{l^3}\cdot r\eta\cdot\phi^{II}\int_0^1(r\eta\cdot\phi^I)^2 d\xi = 0\end{aligned} \tag{3.75}$$

after division of each terms of the former equation by $\widehat{\omega}_1{}^2\cdot(r)$ the following result is obtained

$$\begin{aligned}&\ddot{\eta}\cdot\phi(1+C_a^*) + a_1^*\cdot|r\dot{\eta}\cdot\phi|\cdot\dot{\eta}\cdot\phi + \alpha\frac{1}{\widehat{\omega}_1{}^2 l^4}\cdot\eta\cdot\phi^{IV} - \frac{(\beta+\beta_h(\tau))}{\widehat{\omega}_1{}^2 l^2}\cdot\eta\cdot\phi^{II}\\ &-\frac{\gamma}{\widehat{\omega}_1{}^2 l}\left(\frac{1}{2}-\xi\right)\cdot\eta\cdot\phi^{II} + \frac{\gamma}{\widehat{\omega}_1{}^2 l}\cdot\eta\cdot\phi^{I} - \frac{\mu}{\widehat{\omega}_1{}^2 l^3}\cdot\eta\cdot\phi^{II}\int_0^1(r\eta\cdot\phi^I)^2 d\xi = 0\end{aligned} \tag{3.76}$$

Adopting the Galerkin non-linear method the equation **(3.76)**is multiplied by

$$v(\xi,\eta,\tau) = \delta\left(\frac{W_0(\tau)}{D}\right)\phi(\xi,\eta) = \delta\left(\frac{r}{D}\eta(\tau)\right)\phi(\xi,\eta) \tag{3.77}$$

yielding

$$\ddot{\eta}\cdot\phi^2(1+C_a^*) + a_1^*\cdot|r\dot{\eta}\cdot\phi|\cdot\dot{\eta}\cdot\phi^2 + \alpha\frac{1}{\widehat{\omega}_1{}^2 l^4}\cdot\eta\cdot\phi^{IV}\phi \tag{3.78}$$

$$-\frac{(\beta+\beta_h(\tau))}{\widehat{\omega_1}^2 l^2}\cdot\eta\cdot\phi^{II}\phi-\frac{\gamma}{\widehat{\omega_1}^2 l}\left(\frac{1}{2}-\xi\right)\cdot\eta\cdot\phi^{II}\phi+\frac{\gamma}{\widehat{\omega_1}^2 l}\cdot\eta\cdot\phi^{I}\phi-\frac{\mu r^2}{\widehat{\omega_1}^2 l^3}$$
$$\cdot\phi\phi^{II}\eta\int_0^1(\eta\cdot\phi^I)^2 d\xi=0$$

It should be noted that the coefficients ϕ and its derivatives vary along the riser length. To eliminate such a variation these coefficients will be averaged with respect to the non-dimensional space domain $0\le\xi\le1$ in order to remove the spatial dependence.

$$\ddot{\eta}\cdot(1+C_a^*)\int_0^1\phi^2 d\xi+a_1^*\cdot|r\dot{\eta}\cdot\phi|\cdot\dot{\eta}\cdot\int_0^1|\phi|\phi^2 d\xi+\alpha\frac{1}{\widehat{\omega_1}^2 l^4}\cdot\eta\int_0^1\phi^{IV}\phi d\xi$$
$$-\frac{(\beta+\beta_h(\tau))}{\widehat{\omega_1}^2 l^2}\cdot\eta\int_0^1\phi^{II}\phi d\xi-\frac{\gamma}{\widehat{\omega_1}^2 l}\left(\frac{1}{2}-\xi\right)\cdot\eta\int_0^1\phi^{II}\phi d\xi+\frac{\gamma}{\widehat{\omega_1}^2 l}\cdot\phi\int_0^1\phi^{I}\phi d\xi \qquad \textbf{(3.79)}$$
$$-\frac{\mu r^2}{\widehat{\omega_1}^2 l^3}\cdot\int_0^1\phi^{II}\phi\left(\int_0^1(\eta\cdot\phi^I)^2 d\xi\right)d\xi=0$$

Trying to obtain a handier equation various coefficients are introduced

$A_0=\int_0^1\phi^2 d\xi \quad A_1=\int_0^1\phi^2|\phi|\,d\xi \quad A_2=\int_0^1\phi^{IV}\phi\,d\xi \quad A_3=\int_0^1\cdot\phi^{II}\phi\,d\xi$

$A_4=\int_0^1\left(\frac{1}{2}-\xi\right)\cdot\phi^{II}\phi d\xi \quad A_5=\int_0^1\phi^I\phi d\xi \quad A_6=\int_0^1\phi^{II}\phi\left(\int_0^1(\phi^I)^2 d\xi\right)d\xi$

$\alpha_1=\frac{a_1^*}{(1+C_a^*)} \quad \alpha_2=\alpha\frac{1}{\widehat{\omega_1}^2 l^4(1+C_a^*)} \quad \alpha_3=\frac{\beta}{\widehat{\omega_1}^2 l^2(1+C_a^*)} \quad \alpha_h=\frac{\beta_h}{\omega_1^2 l^2(1+C_a^*)}$ **(3.80)**

$\alpha_4=\frac{\gamma}{\widehat{\omega_1}^2 l(1+C_a^*)} \quad \alpha_5=\frac{\gamma}{\widehat{\omega_1}^2 l(1+C_a^*)} \quad \alpha_6=\frac{\mu r^2}{\widehat{\omega_1}^2 l^3(1+C_a^*)}$

Finally

$$\ddot{\eta}A_0+\dot{\eta}|\dot{\eta}|\alpha_1A_1+\eta\alpha_2A_2-\eta(\alpha_3+\alpha_h)A_3-\eta\alpha_4A_4+\eta\alpha_5A_5-\eta^3\alpha_6A_6 \qquad \textbf{(3.81)}$$

4 CHAPTER 4

In this section the reduced-order model obtained in the previous chapter is resolved using a numerical integration (Dormand–Prince method). With the same technic a different ROM originated from the projection onto a trigonometric function is also solved and compared with the previous one. Finally with the aim of analyzing the quality of the results of the ROMs a FEM model is developed.

4.1 NUMERICAL INTEGRATION OF THE REDUCED ORDER MODEL AND RESULTS

In order to carry out the numerical integration, it is used the software Matlab®. The numerical integration adopted the Dormand–Prince method RKDP an explicit method for solving ordinary differential equations . RKDP is a member of the Runge–Kutta ordinary differential equation solver and is implemented in the Matlab® function ODE45. More specifically, it uses six function evaluations to calculate fourth- and fifth-order accurate solutions and is a one-step solver in computing (t_j) . It needs only the solution at the immediately preceding time point $y(t_{j-1})$.The Dormand–Prince method has seven stages, but it uses only six function evaluations per step because the last stage is evaluated at the same point as the first stage of the next step. The coefficients of the method minimize the error of the fifth-order solution.

Here the fundamental aspects of a Runge-Kutta ordinary differential equation solver are presented. As an example, it is considered the fourth-order Runge-Kutta method.

The method uses a weighted average of the slope evaluated at multiple steps

$$y_{j+1} = y_j + h \sum \gamma_m k_m \tag{4.1}$$

where γ_m are weighting coefficients (In general $\sum \gamma_m = 1$) and k_m are slopes evaluated at points in the interval

$$t_j \leq t \leq t_{j+1} \tag{4.2}$$

The fourth-order Runge-Kutta method computes the slope at four positions within each step

$$k_1 = f(t_j, y_j) \tag{4.3}$$

$$k_2 = f\left(t_j + \frac{h}{2}, y_j + \frac{h}{2}k_1\right) \tag{4.4}$$

$$k_3 = f\left(t_j + \frac{h}{2}, y_j + \frac{h}{2}k_2\right) \tag{4.5}$$

$$k_4 = f(t_j + h, y_j + hk_3) \tag{4.6}$$

It uses weighted average of slopes to obtain

$$y_{j+1} = y_j + h\left(\frac{k_1}{6} + \frac{k_2}{3} + \frac{k_3}{3} + \frac{k_4}{6}\right) \tag{4.7}$$

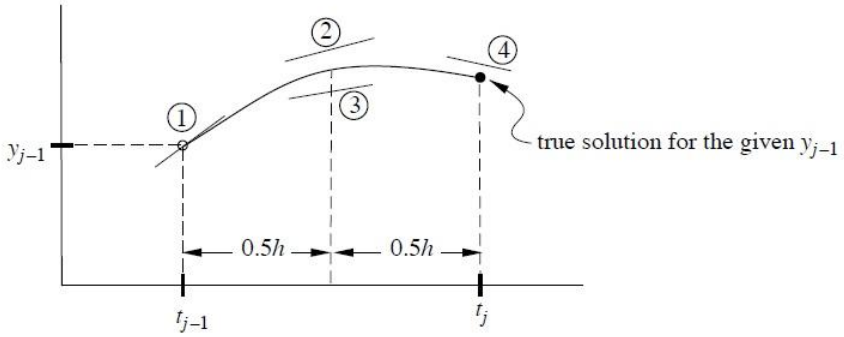

Figure 17: slopes calculation with fourth-order Runge-Kutta method

The numerical predictions are obtained solving the ordinary differential equations according to the procedure already outlined.

The data chosen for the solution of the ROM are the same used in the experimental tests carried out in IPT [10] in order to make the results comparable.

DATA		
Undeformed length	L_0	$2552\ mm$
Stretched length	L	$2602mm$
Immersed length	L_i	$2257\ mm$
Internal diameter	D_i	$15.8\ mm$
External diameter	D	$22.2\ mm$
Riser mass	m	$1{,}190\ kg/m$
Immersed weight	ρ	$7.869\ N/m$
Axial stiffness	EA	$1207\ N$
Bending stiffness	EI	$0.056\ Nm^2$
Average normal force	$\bar{N}$	$23.65\ N$
Fluid density	ρ_{fl}	$1000\ kg/m^3$
Water mass coefficient	C_m	0,3252
Natural frequency in the air	ω_1	$5.7731\ rad \cdot s^{-1}$
Heave amplitude	h_0	$0.025\ m$
Heave frequency	$\widehat{\Omega}$	$10.03\ rad \cdot s^{-1}$

The coefficients $A_0, A_1, A_2, A_3, A_4, A_{5,} A_6$ of equation **(3.81)** are numerically evaluated using adaptive Simpson quadrature.

The coefficient $C_a{}^*$ and C_d are obtained from the calibration fo the ROM to reach a good agreement with the experimental attests carried out at the towing tank[10][11]. In particular, $C_a{}^*$ was obtained by imposing that the first mode natural frequency in still water

$$\hat{\omega}_1 = \frac{\omega_1}{\sqrt{1 + {C_a}^*}}$$

should be equal to the experimental value $\hat{\omega}_1 = 5{,}015 \left[\frac{rad}{s}\right]$

The results here presented are based on the drag coefficient value equal to

$$C_d = 2.84$$

That is good agreement with the paper [12] that proposes

$$C_d = 2.946$$

Using the linearized Bessel-like first mode as the projection function within the Galerkin method, the following results in terms of amplitude, phase portrait and power spectral density are obtained. The results comes out from the numerical integration of the equation **(3.81)** which is a dimensionless equation and then even the graphs presented are accordingly dimensionless

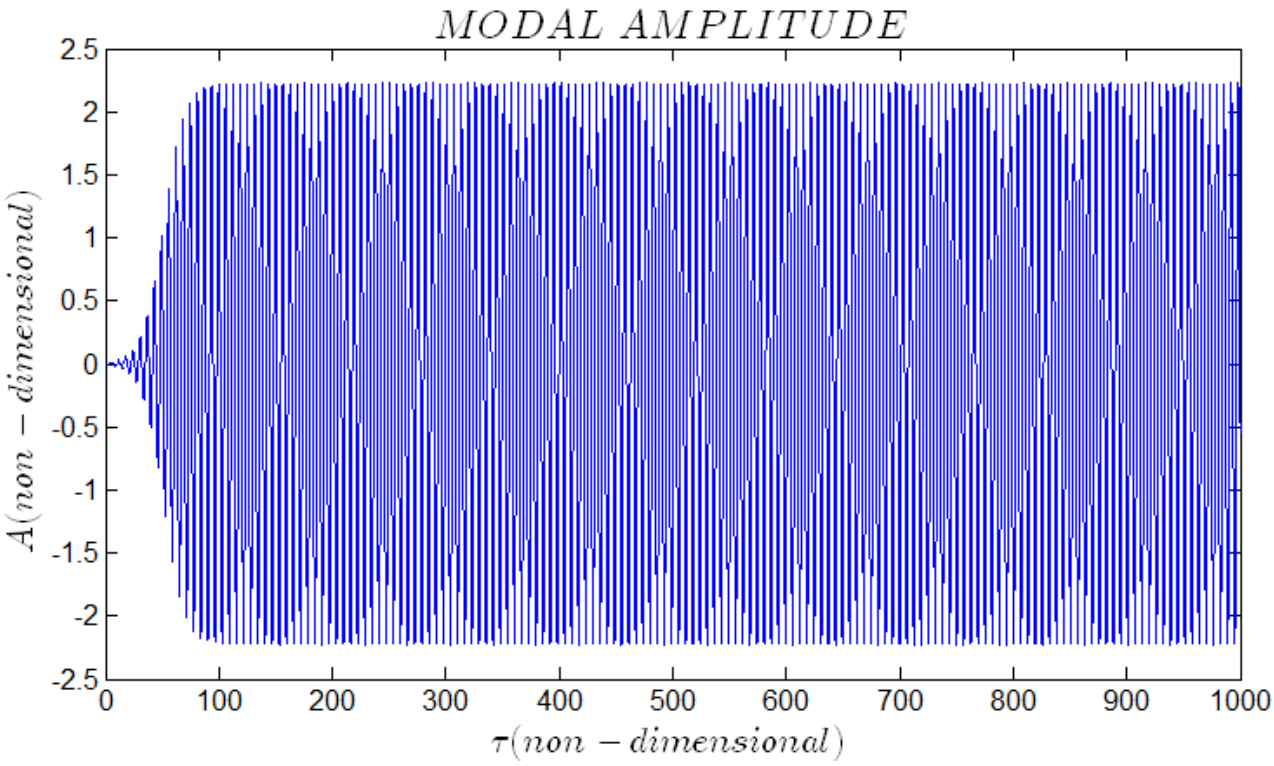

Figure 18: Non-dimensional modal amplitude ROM (Bessel-like)

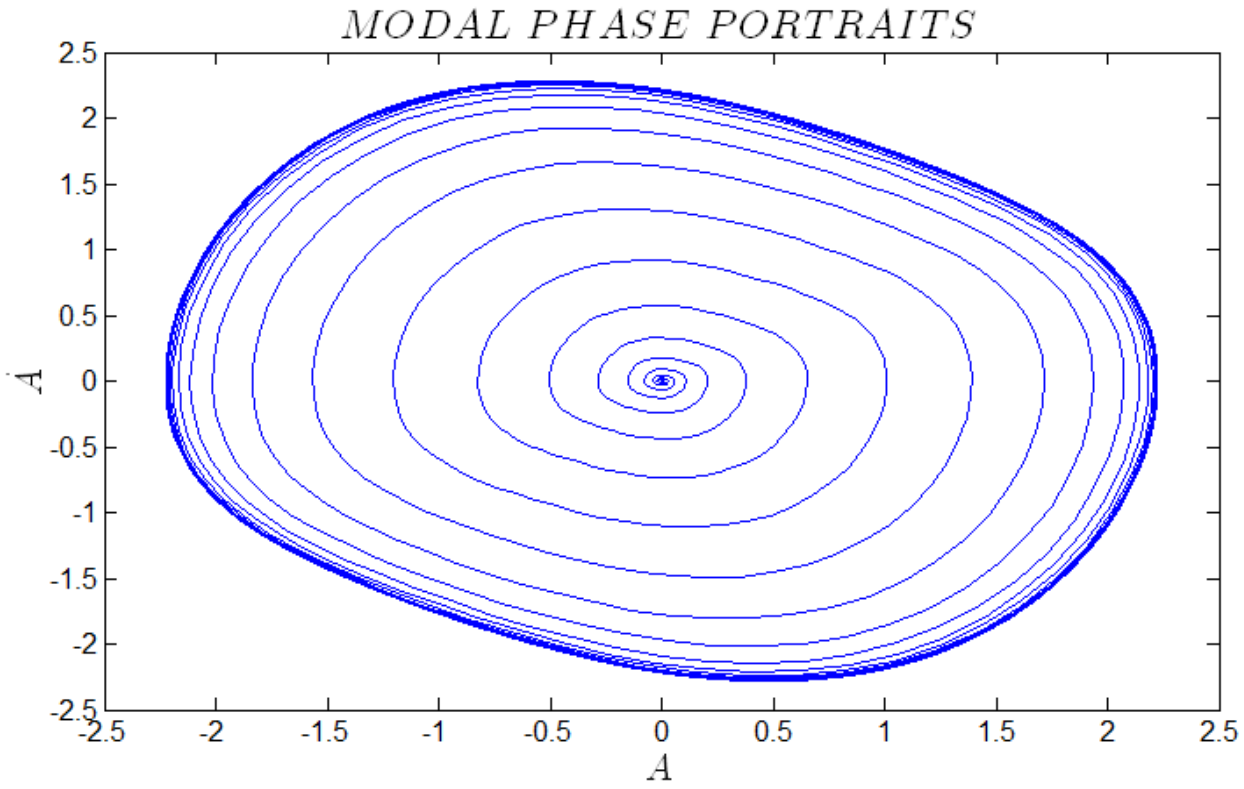

Figure 19: Modal phase portrait ROM(Bessel-like)

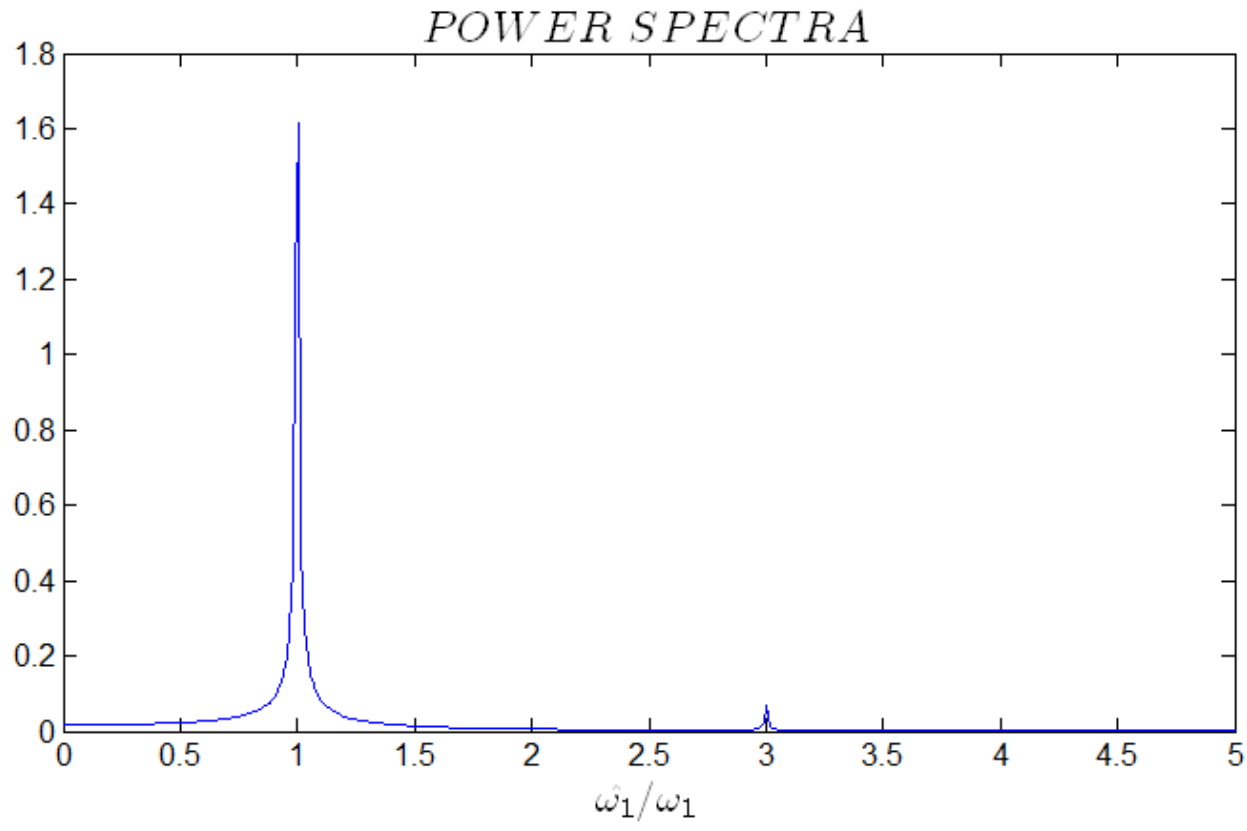

Figure 20: Power spectra ROM (Bessel-like)

Remembering that the equation was non-dimensionalized also with respect to the gyration radius $r = \sqrt{\frac{I}{A}} = 0.0068[m]$ and the maximum (non-dimensional) amplitude recorded is $A = 2.2239$, we finally get a dimensional amplitude of $A_d = 0.0151\ [m]$ that is equal to the same as the amplitude obtained in the IPT test [10].

The spanwise distribution of the Power Spectrum Density doesn't show a perfect peak at 1 because the natural frequency of the first mode $\omega_1 = 5{,}7731\ [\frac{rad}{s}]$.

One of the scopes of this work is also to prove that a reduced-order model obtained by means of a non-linear mode provides better results in comparison with a MOR originated from the projection onto a trigonometric function [12] as

$v_k = A_k \sin(k\pi\xi)$	**(4.8)**

Where $k = 1,2,3 \ldots n$ is the number of modes considered

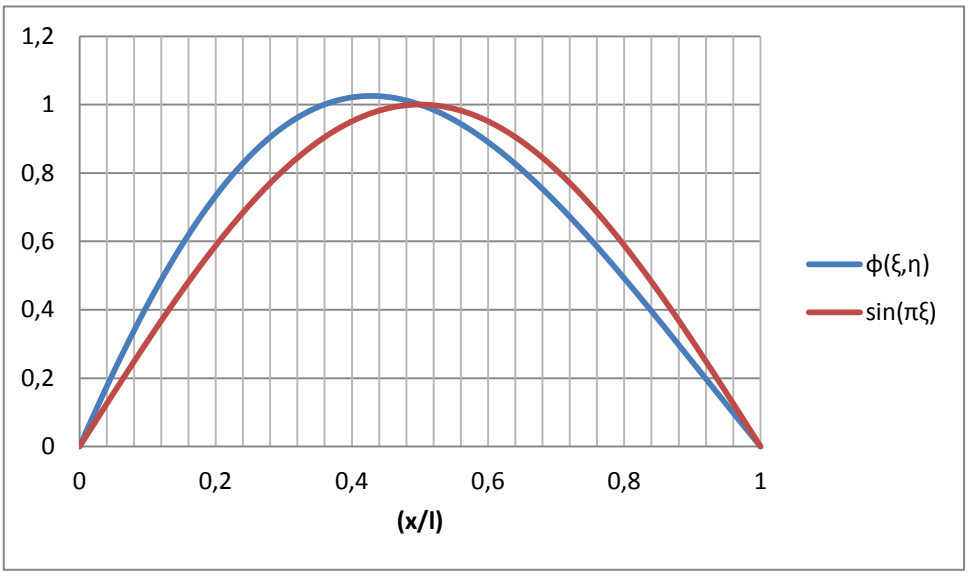

Figure 21: Bessel-like mode vs. trigonometric mode

To prove that the analysis is repeated with the same data and the same model (of course with $v_k = A_k \sin(k\pi\xi)$instead of non-linear mode) and the results are show in the Figures 22-23-24.

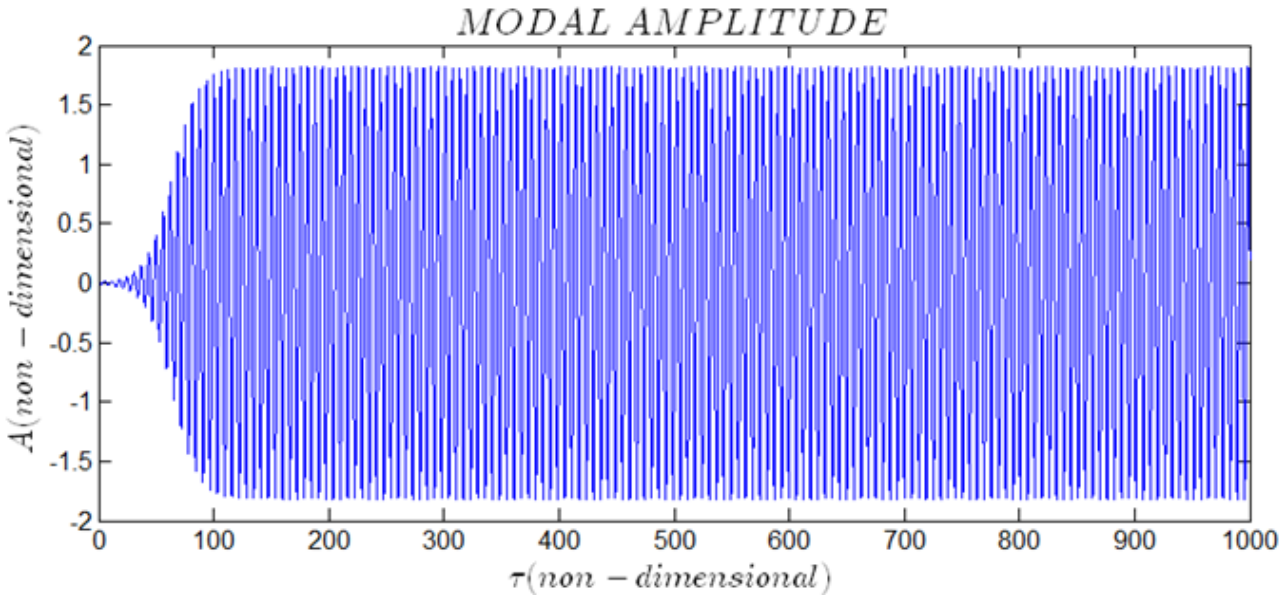

Figure 22: Non-dimensional modal amplitude ROM (trigonometric-like)

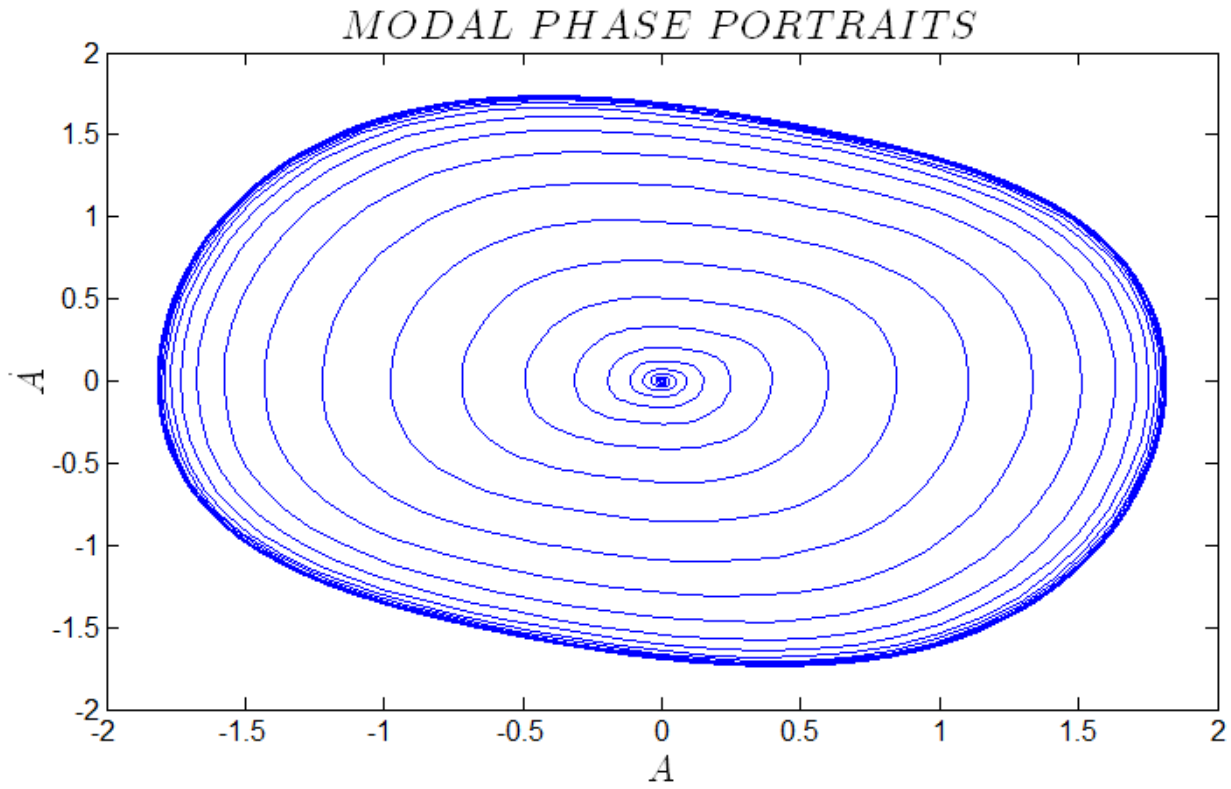

Figure 23: Modal phase portrait ROM (trigonometric-like)

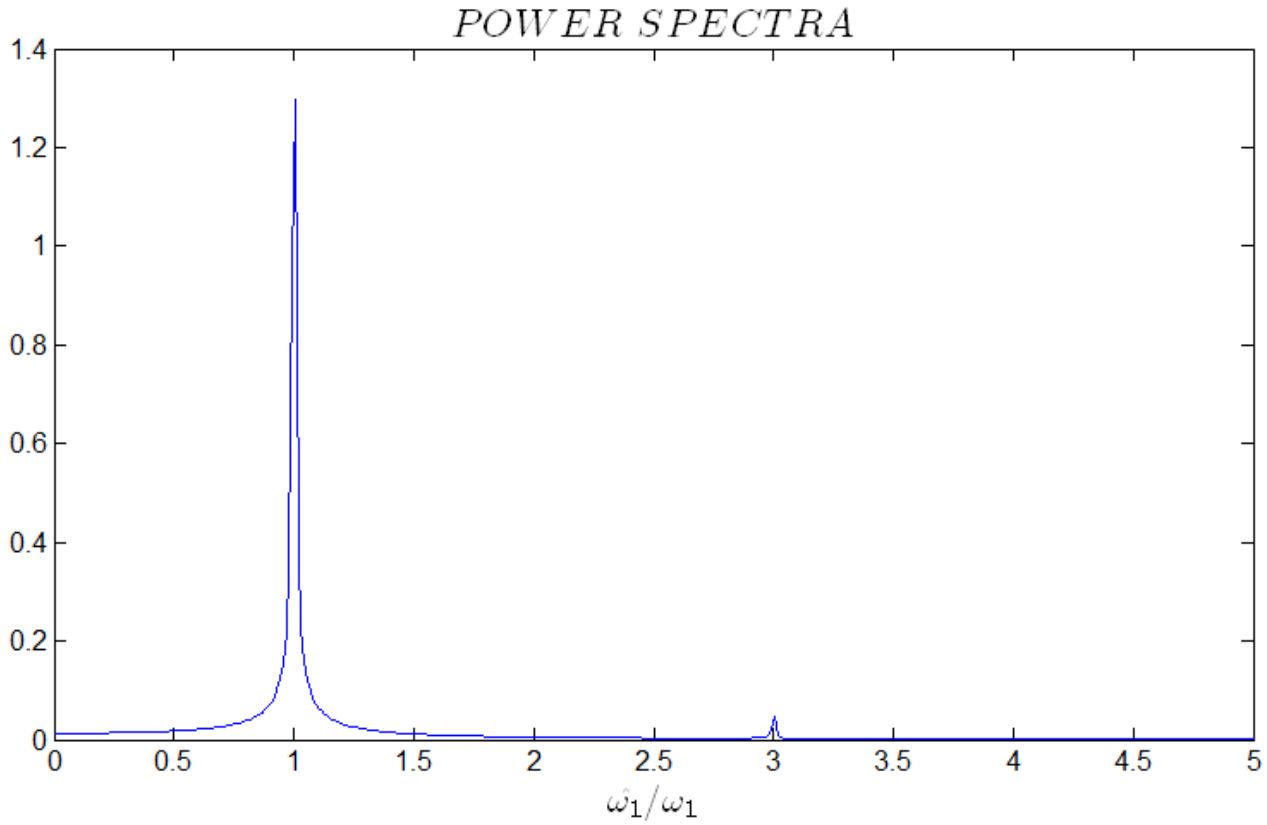

Figure 24: Power spectra ROM (trigonometric-like)

The non-dimensional amplitude is significantly reduced $A = 1.8148$ namely $-18{,}40\%$. In order to obtain a result close to the experimental one ($A_d = 0.015\ [m]$) the drag coefficient ${C_a}^*$ should be posed equal to

$$ {C_a}^* = 2.25 $$

The results of this section clearly show that: despite of the slightly difference between the two functions (Bessel-like and trigonometric) used for projecting via Galerkin method the continuum dynamics system such a difference can strongly affect the precision of the analysis.

Although the two types of functions are initially similar (Fig. 21), in the ROM's equation **(3.81)** appear coefficients related to their derivatives up to the fourth order and for each derivation the difference between the two functions increase and consequently also the ROM's results are affected.

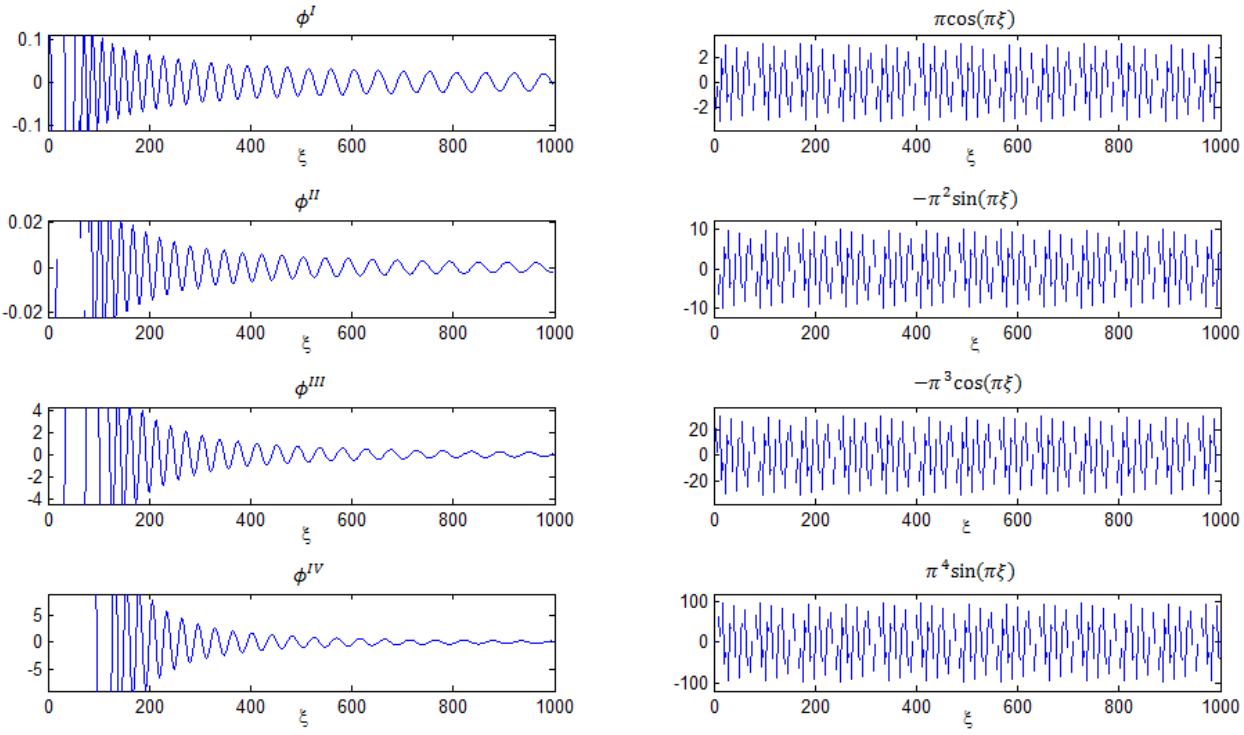

Figure 25: Bessel-like derivatives vs. trigonometric derivatives

Furthermore it was shown haw the drag coefficient is a key parameter for the reduced-order model here proposed and a little variation of this parameter has a strong effect on the ROM.

4.2 FINITE-ELEMENT ANALYSIS WITH A DEDICATED CODE

In order to have another mean of comparison for the ROM's result, a finite element analysis of the vertical riser subjected to heave is carried out with dedicated software. OrcaFlex® is a marine dynamics program developed by Orcina for static and dynamic analysis of a wide range of offshore systems, including the rigid risers.

The equation of motion which OrcaFlex® solves is as follows:

$$M(p,a) + C(p,v) + K(p) = F(p,v,t) \tag{4.9}$$

where

$M(p,a)$ is the system inertia load.

$C(p,v)$ is the system damping load.

$K(p)$ is the system stiffness load.

$F(p,v,t)$ is the external load.

p is the position and v velocity and acceleration vectors respectively.

t is the simulation time.

The schema re-evaluates the system geometry at every time step and so the simulation takes full account of all geometric non-linearities, including the spatial variation of both wave loads and contact loads.

The finite element model for a line implemented in OrcaFlex® consists in a model divided into a series of line segments which are then modeled by straight massless model segments with a node at each end as shown in the figure below

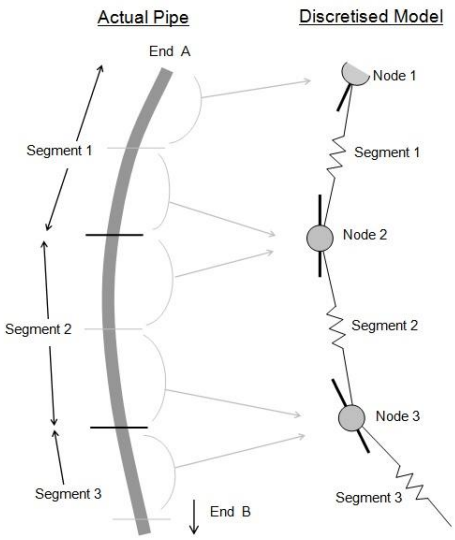

Figure 26: Orcalex fem element

The riser is first modeled so as to obtain normal forces that in the static analysis are close to the normal forces of the IPT test [1], namely:

$$\text{Static tension at the top } N_t(0) = 33{,}88\ [N]$$

$$\text{Static tension at the bottom } N_b(0) = 13{,}41\ [N]$$

with a linear variation

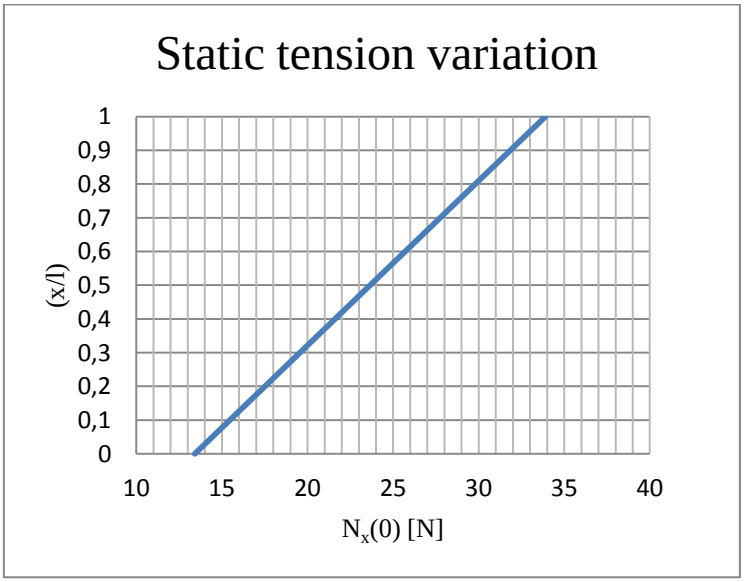

Figure 27: Static tension variation

To achieve this goal the length of the riser is calibrated since the normal force is given by its elongation. The length (before stretching was applied) which allows to have the same static tension distribution is

$$L = 2552\, mm$$

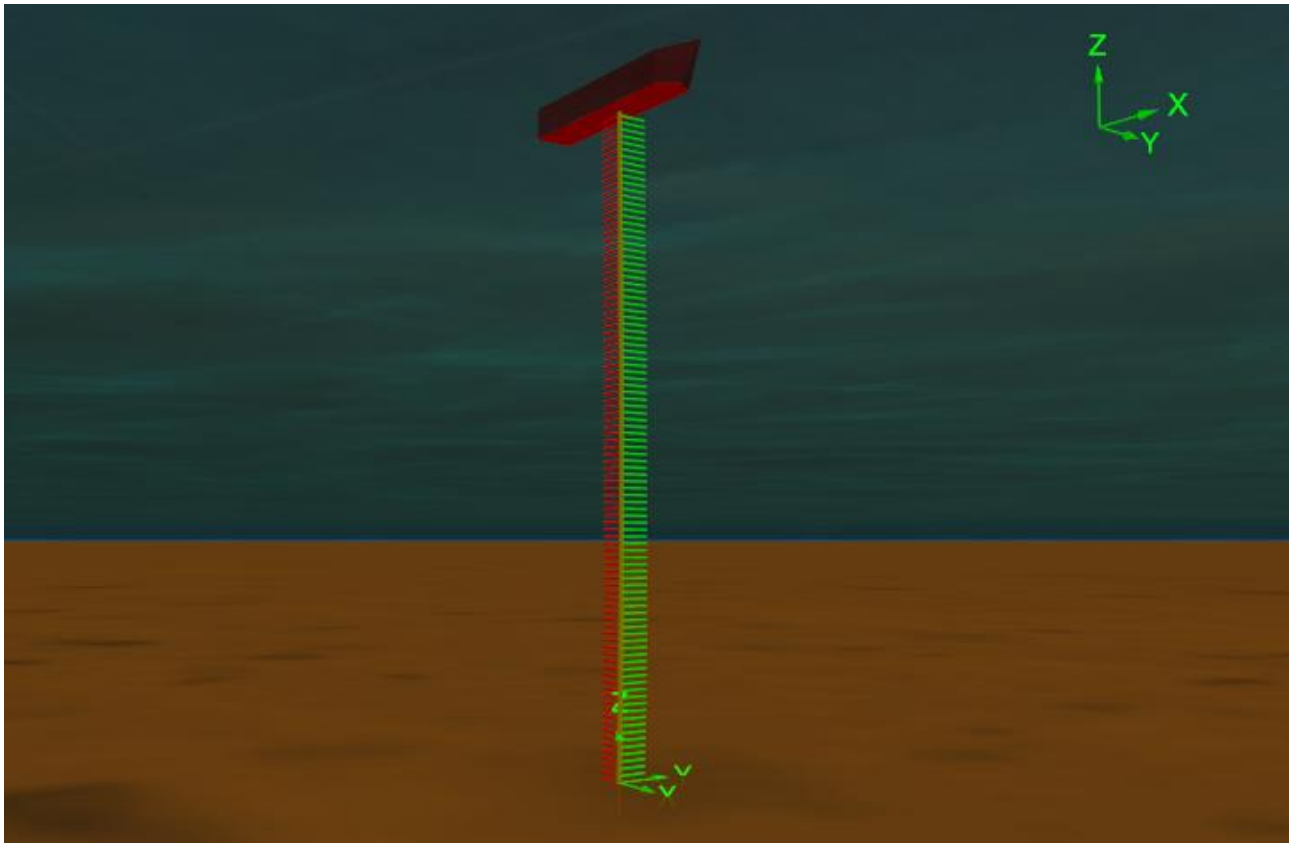

Figure 28: Orcalex model

OrcaFlex® calculates hydrodynamic loads on risers using an extended form of Morison's Equation [13] and setting the data already used in the previous section we get the following results (Fig. 29-30)

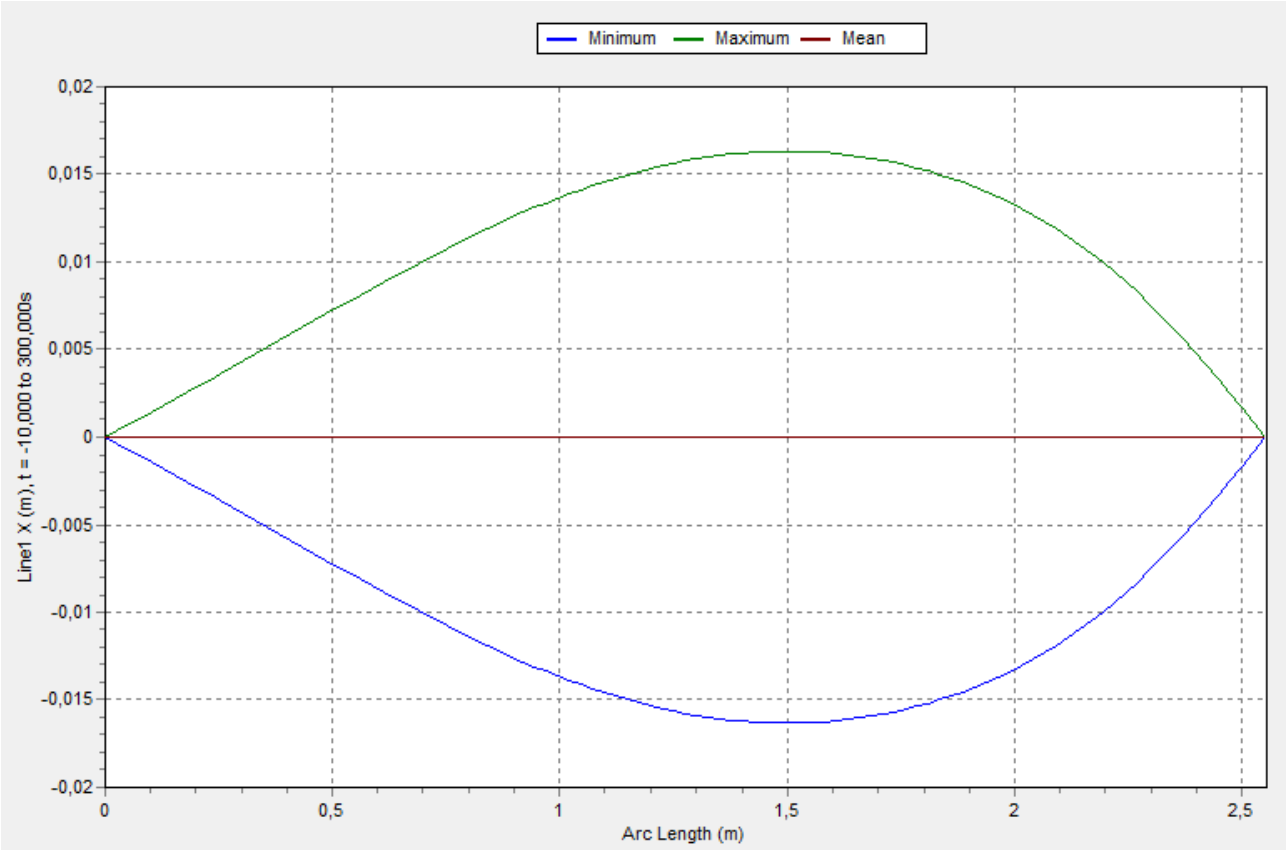

Figure 29: Modal shape

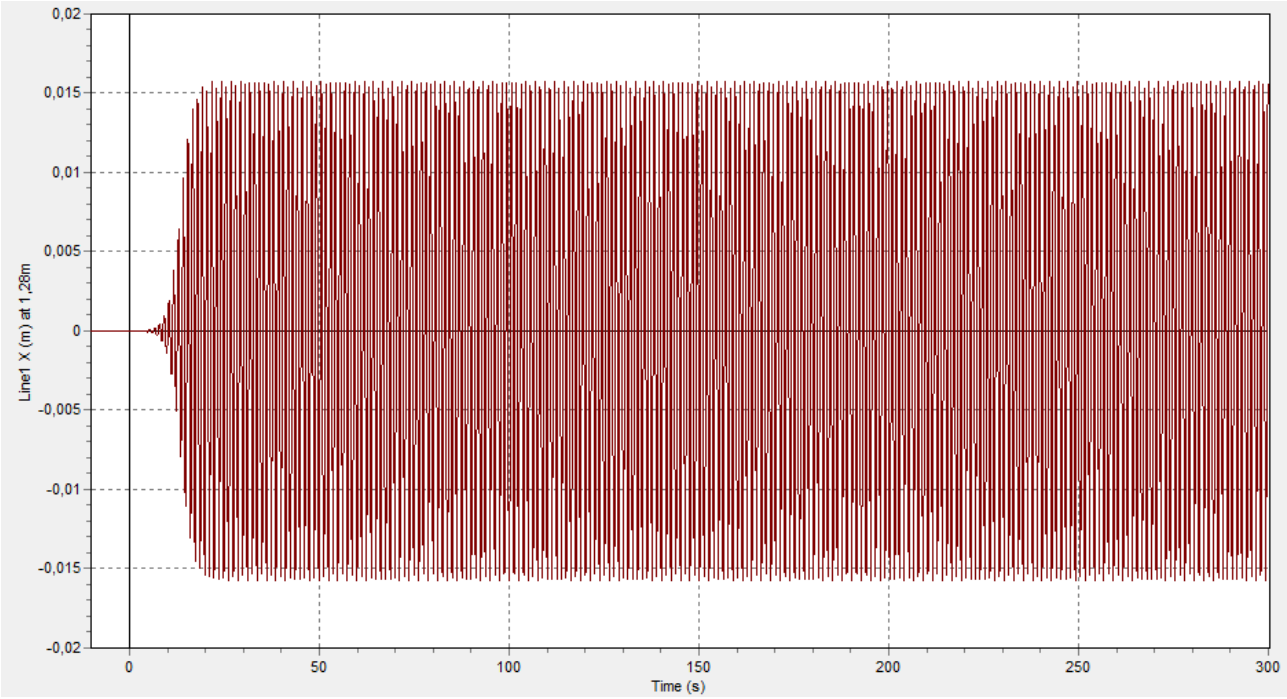

Figure 30: Modal amplitude at the mid-span

Amplitude in in meters and referred to the mid-span where approximately the amplitude reach the maximum.

It can be noticed that the model predicted an amplitude $A = 0{,}016\ [m]$ close to the Bessel-like ROM. It must be underlined that OrcaFlex® compute the same shape already given by the Bessel-like mode and not a trigonometric sinusoidal function confirming the greater accuracy of ROM obtained by a projection onto a Bessel-like mode.

5 CONCLUSION

The objective of this thesis was to create a reduced-order model able to predict the behavior of a vertical rigid riser subjected to vertical or the length before stretching was applied top motion (heave) with a frequency twice of the natural one in order to study the parametric resonance phenomenon. The behavior's correct prediction of the riser under such excitation can help to avoid some important problems especially the one related to fatigue. Firstly, the vertical riser was studied as an axially loaded beam assuming the classic hypothesis of Euler-Bernoulli theory and by using the Hamilton's principle it was possible to obtain the non-linear equation of motion. Starting from the previously obtained equation and introducing some approximations (single-mode dominated dynamics, Galerkin temporal projection, non-linear correction in the normal force) it was possible to get the non-linear Bessel-like vibration modes. The results have shown that for the first mode (and only for the first) the non-linear correction previously introduced can be neglected without compromising the quality of results. The first Bessel-like mode was then used as the projection function within the non-linear Galerkin method in order to obtain the ROM. Once the analytical expression of ROM was obtained, the amplitudes of the response were analyzed via numerical integration (Dormand–Prince method).After that different comparisons were made to ensure the reliability of the reduced model. The first and most important comparison was carried out with the experimental results obtained with a physically-reduced model tested at the towing tank of IPT. The ROM was in fact developed directly over the data obtained experimentally, yet requiring a calibration of the natural frequency is still water (through coefficient $C_a{}^*$) and the drag coefficient to reach a good agreement with the experimental results.

One of the main goals of the project was to analyze if the ROM obtained via projection on a Bessel-like would provide better results, in terms of quality and time demand, compared to a ROM based on a trigonometric function. For this purpose two analyses with the two different ROMs with the some data were carried out. The results have indicated that between the two models there is a remarkable difference in the amplitude estimation (difference of 18,4%).

However it must be underlined that the drag coefficient used in this comparison was the one obtained after calibration on the base of the ROM with Bessel-like and is clearly for this that the ROM(Bessel-like mode) perfectly fits the experimental results unlike the other model.

To ensure the quality of the result of the ROM(Bessel-like mode) a finite element analysis with a dedicated software was performed. This analysis has shown that the shape and even the amplitudes of the FEM model are more in accordance with the ROM(Bessel-like mode) that with the ROM (trigonometric function) which underestimates the amplitudes and has a sinusoidal shape.

The purpose of the thesis seems to have been reached. Obtain and analyze a ROM (Bessel-like mode) implies a greater mathematical effort in comparison to a ROM (trigonometric-like mode) but the quality of the results justifies the choice.

6 BIBLIOGRAPHY

1. *On the existence of normal mode vibrations in nonlinear system.* **C.H. Pak, R.M. Rosenberg,**1968,Q. Appl. Math. 26.

2. Normal modes for non-linear vibratory systems. **S.W. Shaw, C. Pierre**, 1993, Journal of Sound and Vibration, 164: 85-124.

3. *An analysis of parametric instability of risers.* **F.S. Prado,F.Y. Sakamoto,C.E.N. Mazzilli,**2014, Latin American Journal of Solid and Structure, 11: 348-368.

4. *Nonlinear Oscillations.* **A.H. Nayfeh, D.T. Mook,** 1979,Wiley.

5. *Reduced-order modelling in non-linear dynamics: an approach based on nonlinear normal mode.***C.E.N. Mazzilli, G. C. Monticelli, N. A. Galan Neto**,2011,Journal of Mechanical Engineering Science, 225: 2354-2368

6. *Non-linear reduced-order modeling of vortex-induced vibration in straight risers.* **C.E.N. Mazzilli, R. Poncet,** 2012,Pan-American Congress of Applied Mechanics, Port of Spain.

7. *Non-linear modal analysis for beams subjected to axial loads: Analytical and finite-element solutions.* **C.E.N. Mazzilli, C.T. Sanches, O.G.O. Bracho Neto, M. Wiercigroch, M. Keber.** 2008, International Journal of Non-Linear Mechanics, 43:551-561.

8. *Effect of linearly varyng normal force upon the nonlinear modal analysis of slender beams.* **C.E.N. Mazzilli,**2008,ENOC Saint Petersburg.

9. *Non-linear free vibrations of tensioned vertical risers.* **C.E.N. Mazzilli,** 2014,ENOC, Vienna.

10. *Experimental analysis of a vertical and flecible cylinder in water:response to top motion excitation and parametric resonance.* **G. R. Franzini, C. Pesce,R. Salles,R.T Gonçalves,A.L.C. Fujarra,P. Mendes** ,2014 ,ASME 33rd International Conference on Ocean Offshore and Artic Engineering,San Francisco.

11. *Risers Model Tests: Scaling Methodology and Dynamic Similarity.* **F. Rateiro, C. Pesce, R.T Gonçalves,G. R. Franzini, A.L.C. Fujarra, R. Salles, ,P. Mendes,**2012**,** International Offshore and Polar Engineering Conference,Rhodes.

12. *Interaction between VIV and heave-imposed motion in vertical risers: a case of study leading to chaotic response?* **Franzini, Guilherme.**

13. *OrcaFlex Manual.* www.orcina.com/SoftwareProducts/OrcaFlex/Documentation/OrcaFlex.pdf,2012.